Gut microbiota promotes enteroendocrine cell maturation and mitochondrial function

Alfahdah Alsudayri[1], Shane Perelman[1], Annika Chura[1], Melissa Brewer[1], Madelyn McDevitt[1], Catherine Drerup[2], Lihua Ye[1]*

1 Department of Neuroscience, the Ohio State University Wexner Medical Center

2 Department of Integrative Biology, University of Wisconsin-Madison

Abstract

The enteroendocrine cells (EECs) in the intestine are crucial for sensing ingested nutrients and regulating feeding behavior. The means by which gut microbiota regulates the nutrient-sensing EEC activity is unclear. Our transcriptomic analysis of the EECs from germ-free (GF) and conventionalized (CV) zebrafish revealed that commensal microbiota colonization significantly increased the expression of many genes that are associated with mitochondrial function. Using in vivo imaging and 3D automated cell tracking approach, we developed new methods to image and analyze the EECs' cytoplasmic and mitochondrial calcium activity at cellular resolution in live zebrafish. Our data revealed that during the development, shortly after gut microbiota colonization, EECs briefly increased cytoplasm and mitochondrial Ca^{2+}, a phenomenon we referred to as "EEC awakening". Following the EEC awakening, cytoplasmic Ca^{2+} levels but not mitochondrial Ca^{2+} level in the EECs decreased, resulting in a consistent increase in the mitochondrial-to-cytoplasmic Ca^{2+} ratio. The increased mitochondrial-to-cytoplasmic Ca^{2+} ratio is associated with the EEC maturation process. In immature EECs, we further discovered that their mitochondria are evenly distributed in the cytoplasm. When EECs mature, their mitochondria are highly localized in the basal lateral membrane where EEC vesicle secretion occurs. Furthermore, CV EECs, but not GF EECs, exhibit spontaneous low-amplitude calcium fluctuation. The mitochondrial-to-cytoplasm Ca^{2+} ratio is significantly higher in CV EECs. When stimulating the CV zebrafish with nutrients like fatty acids, nutrient stimulants increase cytoplasmic Ca^{2+} in a subset of EECs and promote a sustained mitochondrial Ca^{2+} increase. However, the nutrient induced EEC mitochondrial activation is nearly abolished in GF zebrafish. Together, our study reveals that commensal microbiota are critical in supporting EEC mitochondrial function and maturation. Selectively manipulating gut microbial signals to alter EEC mitochondrial function will provide new opportunities to change gut-brain nutrient sensing efficiency and feeding behavior.

Introduction

Feeding behavior is conserved among all organisms. During development, the fetus receives its nutrient supply from its mother. Immediately after birth, the maternal nutrient supply is cut off and the infant needs to initiate the feeding process to obtain nutrients. After eating, the ingested nutrients need to be sensed, and such nutrient information will be transmitted to the rest of the body to coordinate its metabolic function [1]. Within the

intestinal epithelium, a group of specialized sensory cells called enteroendocrine cells (EECs) sense the ingested nutrient information and secrete hormone molecules to regulate physiological homeostasis [2]. The EECs are critical nutrient sensors in the intestinal epithelium. They are dispersed along the digestive tract and comprised of less than 1% of the intestinal epithelium cells (IECs). However, collectively, the EECs form the largest endocrine organ in the body [2]. Most of the previous studies assessing EECs are focused on adults. It is well-known that ingested nutrients, such as fatty acids or glucose, directly stimulate the EECs by triggering a cascade of membrane depolarization, action potential firing, voltage-dependent calcium entry, and hormone-containing vesicle release [2]. Many of these EEC-secreting hormones, like Cholecystokinin (CCK) or glucagon-like peptide 1 (GLP-1), are critical in regulating satiation response and metabolism [1, 2]. In addition to the classic hormone secretion function, recent research also demonstrated that the EECs form a basal membrane process called “neuropod” that directly synapses with the vagal sensory neurons [3, 4]. Through the EEC-vagal neuronal pathway, ingested nutrient information in the gut lumen can be transmitted to the brain [4]. Further studies demonstrated that this nutrient-sensing EEC-vagal pathway is essential to drive animal’s food preference toward sugar and fat [5-7]. It is well known that the intestinal epithelium cells undergo significant remodeling during the postnatal period to adapt to the need for nutrient absorption and sensation [8]. Despite the importance of EECs in nutrient monitoring, gut-brain nutrient sensing, feeding behavior, and systemic metabolic regulation, little is known about how environmental factors regulate EEC maturation and function during the postnatal developmental period.

Following birth, newborn babies are rapidly colonized by microbial organisms [9]. These microbial organisms start to assemble the functional microbial community that plays important roles in the development of the infant [9]. Previous studies revealed that microbiota colonization during the early postnatal phase is critical in promoting intestinal epithelium maturation and remodeling [10-12]. Numerous pieces of evidence also suggest that gut microbiota are important in regulating nutrient absorption, metabolism, and infant growth [13-15]. Research from animal models and clinical studies suggest that gut microbiota are critical in modulating feeding behavior, including appetite and food choice [16]. However, little is known about how gut microbiota interacts with EECs and regulates the EECs' function. Whether and how gut microbiota interacts with EECs to modulate postnatal physiological homeostasis remains unknown.

Mitochondria is the essential organelle that provides ATP to sustain cellular function. The mitochondria emerge as a key player in coordinating cellular metabolism, cell differentiation, and regulating intestinal epithelium homeostasis [17-19]. In the nervous system, mitochondria are important in supporting neuronal vesicle secretion, neuronal synaptic transmission, and neuronal network formation [20]. Research in pancreatic endocrine cells also revealed that mitochondrial function is essential for pancreatic beta-cell hormonal secretion [21]. Interestingly, the pancreatic islet’s mitochondrial activity is inhibited in diabetic conditions [21, 22]. Little is known about the physiological roles of the mitochondrial function in EECs, and how environmental factors regulate EEC mitochondrial activity *in vivo*.

A major challenge in studying how environmental factors, such as gut microbiota, regulate EEC physiology has been the lack of in vivo techniques to study this rare intestinal epithelium population in the intact animal setting. Historically, these cells have been studied by measuring the circulating EEC-secreting hormones [2]. However, many EEC hormones have very short half-lives and the plasma hormone level does not mirror the EEC function nor the real-time EEC activity [23]. EEC activity has also been studied via cell culture or organoid culture systems. However, a cell or organoid culture is not able to mimic the dynamic and complex intestinal luminal factors that shape the EECs. It is also difficult to study how EECs communicate with neighboring cells or distant organs, like the brain, using the in vitro culture system.

In this study, we utilized the zebrafish model to examine how commensal microbiota affect EEC maturation and function. Using an innovative approach to direct images and track the EEC cellular and mitochondrial calcium activity in live zebrafish during development, our results revealed that the EEC morphology, cellular, and mitochondrial activity is dynamically regulated during the EEC maturation process. Importantly, our results revealed that gut microbiota play critical roles in promoting EEC maturation and mitochondrial function.

Results

Gut microbiota alters EEC subtypes

Previous studies, including ours, demonstrated that similar to mammals, the zebrafish EECs have diverse subtypes [24, 25]. A recent zebrafish intestine epithelium single-cell RNA sequencing dataset further revealed the five EEC subtypes in the zebrafish larvae characterized by their distinct hormone expression profiles (Fig. S1A-B) [26]. EEC1 is characterized by the expression of the hormonal genes: pancreatic polypeptide b (*pyyb*), somatostatin 2 (*sst2*), and ghrelin (*ghrl*) (Fig. S1A-B). EEC2 expresses the hormonal genes: preproglucagaon a (*gcga*), the gene that encodes Glucagon (Gcg) or Glucan-like-pepetide 1 (GLP-1), vasoactive intestinal polypeptide b (*vipb*), and insulin-like 5 (*insl5*) (Fig. S1A-B). EEC3 expresses the hormonal genes: calcitonin related polypeptide alpha (*calca*) and neuromedin b (*nmb*) (Fig. S1A-B). EEC4 expresses the hormonal genes: cholecystokinin a (*ccka*) (Fig. S1A-B). EEC5 uniquely expresses the following hormonal genes: brain-derived neurotrophic factor (*bdnf*), adenylate cyclase-activating peptide-1 a (*adcyap1a*), preproenkephalin a (*penka*), and tryptophan hydroxylase 1 b (*tph1b*), the enzyme that synthesizes serotonin (Fig. S1A-B). The EEC5 also highly and uniquely expresses the Transient receptor potential ankyrin 1 b (Trpa1b). These Trpa1+EECs that are characterized in our previous studies sense microbial stimulants and are critical in regulating gut motility and intestinal homeostasis [27]. Some of these EEC markers can be labeled via immunofluorescence staining and transgenic approaches (Fig.S1C-K). Our results confirmed the hormonal expression profiles in different EEC subtypes that are revealed in the single-cell RNA sequencing above (Fig. S1C-K). Moreover, consistent with previous studies, our data revealed that the distribution of the EEC subtypes exhibits regional specificity (Fig. S1C-K). For example, the PYY+EECs are exclusively in the proximal intestine, while the Trpa1+EECs are distributed along the whole digestive tract. Interestingly, the Trpa1+EECs (EEC5) appeared to have heterogeneity. As the proximal

intestinal Trpa1+EECs express both Enk and Serotonin (Fig. S1C-K). However, the middle and distal intestinal Trpa1+EECs do not express ENK but only express serotonin (Fig. S1C-K).

Next, we investigated how commensal gut microbiota affect EEC subtype specification via the zebrafish gnotobiotic approach (Fig. 1A) [28]. The zebrafish were derived as germ-free at 0 day post fertilization (dpf) [28]. At 3dpf, the zebrafish are maintained as germ-free (GF) or colonized with commensal microbiota (Conventionalized, CV). The gnotobiotic zebrafish were fed from 3dpf to 7dpf, and the zebrafish were fixed at 7dpf for immunofluorescence staining. Our results revealed that commensal microbiota colonization did not significantly alter the percentage of PYY+ EECs and ENK+EECs in the proximal intestine (Fig. 1B-E', J-K). However, commensal microbiota colonization decreased the number of Gcg/GLP-1+EECs in the proximal intestine and Trpa1+EECs in the distal intestine (Fig. 1F-I, L-N).

Gut microbiota promotes EEC maturation and mitochondrial function

To further understand how commensal microbiota modulate EECs in zebrafish, we used Flow Activated Cell Sorting (FACS) to isolate EECs from GF and CV zebrafish and performed transcriptomic analysis (Fig. 2A). For each gene, the fold change in response to gut microbial status (CV vs GF) and fold change in response to the cell fate (EEC vs other IEC) was plotted (Fig. 2B). Our results demonstrated that there is a weak but significant positive correlation between genes that are enriched in EECs and the genes that are upregulated in the CV condition(Fig. 2B). Within the genes that are significantly upregulated in CV, about 74.5% of them are enriched in the EECs (Fig. 2C). We then plotted the conserved EECs' signature genes that are shared among zebrafish, mice, and humans [27] (Table 1). Our results indicate that about 72% of those conserved EEC signature genes are upregulated in CV (Fig. 2D, Table 1). Within those conserved EEC genes, many of them are associated with EEC cell membrane potential regulation and vesicle secretion (Fig. 2E). The CV condition also significantly upregulates the chromogranin A gene (*chga*), which labels the mature EECs (Fig. 2E)[29]. Therefore, consistent with the immunofluorescence results above, the transcriptomic analysis indicates that gut microbiota promote EEC cell fate and maturation. Next, we performed Go Term analysis of the genes that are significantly upregulated in CV and the genes that are significantly upregulated in GF using the Metascape gene analysis tool (Fig. 2F-G). Interestingly, in the genes that are significantly upregulated in GF EECs, top Go Term includes gene functions related to adhesion, migration, and actin filament-based processes (Fig. 2G). Within the CV upregulated genes, several Go Terms associated with mitochondrial function are enriched (Fig. 2G).

Next, we annotated all of the genes associated with different aspects of mitochondrial function (Table). We found that almost all of the genes in the FASTK mitochondrial RNA binding family, TIM23 complex, and mitochondrial contact site and cristae organizing system are upregulated in CV (Table 1). The mitochondrial DNA encodes 13 proteins that are critical for electron transport chain reactions [30]. The FAS-activated serine/threonine kinase family (FASTK) is located in the mitochondrial matrix and plays an important role in processing RNA transcribed from the mitochondrial DNA [31]. The FASTK gene family

is essential for synthesizing the components of the electron transport chain [31]. Within the FASTK family, previous studies showed that FASTK and FASTKD2 increase the NADH dehydrogenase transcripts and promote mitochondrial respiration specifically [31, 32]. FASTKD2 is one of the most significant genes upregulated in CV EECs (Fig. 2H). Mitochondria acquire most of their protein from the cytosol [33]. The TIM23 complex is essential for translocating cytosolic preprotein into the mitochondrial matrix across the mitochondrial membrane [33]. Within the mitochondria, the inner membrane forms invaginations known as cristae. The cristae are very specialized structures that support respiration [34]. Our results indicate that many genes that are associated with cristate organization are upregulated in CV EECs (Table1), suggesting that commensal microbiota colonization increases EEC mitochondrial respiration function. In addition to the genetic pathways above, our results also indicate that cox10 (an important component of mitochondrial respiration for complex III) is among the most significantly upregulated CV EEC genes (Fig.2H). Together, our transcriptomic data indicates that gut microbiota promote EEC maturation and mitochondrial function by increasing different genetic pathways that are involved in mitochondrial respiration (Fig. 2I).

Immature EECs contain active filopodia structures at the basal lateral membrane.

Our RNA sequencing results revealed that GF zebrafish exhibit increased gene expression related to their actin filament. We then used a *Tg(neurod1:lifeActin-EGFP)* transgenic zebrafish model [24] to examine EEC actin filament dynamics. The 3dpf and 6dpf proximal intestines of the fixed zebrafish samples were examined. The zebrafish EECs start to form at around 60 hours post fertilization. At around 3dpf, the zebrafish hatched from their chorion. The gut lumen opens and gut microbiota starts to colonize the intestine. Previous studies demonstrated that the intestinal epithelium cells, including EECs, are highly polarized and contain a dense actin network in the microvilli at the apical brush border [24]. To our surprise, our data showed that at 3dpf, almost all of the zebrafish EECs exhibit complex actin filament protrusions at the base (Fig. 3A-A'). Interestingly, we did not detect active basal actin filament in other IECs at 3dpf zebrafish (Video 1). This indicates that the formation of the basal actin filaments is not associated with the general intestinal epithelium development process. It is a unique phenomenon that involves immature EECs. By 6dpf, the EECs' basal actin filaments disappeared. Most EECs exhibited typical spindle-type morphology with a flat base (Fig. 3B-B'). To further examine the EEC actin filament dynamic change, we performed live imaging of the EECs at 3dpf *Tg(neurod1:lifeActin-EGFP)* in zebrafish and traced the same fish to 6dpf. Consistently, we observed that at 3dpf, almost all the EECs have complex actin filopodium filaments in the basal lateral portion, and the EEC extends and retracts their filopodium filaments constantly (Fig. 3C-D') (video 2). However, in the same zebrafish, by 6dpf, the EECs do not have actin filaments at the base but contain a high lifeActin-EGFP signal at the apical brush border (Fig. 3E-F') (video 3). Our data revealed for the first time that the immature EECs have an active filopodia process at the basal lateral membrane. When the EECs start to develop and mature, they become more polarized and lose their basal filopodia process. In general, filopodia are an antenna for cells to probe their environment [35]. The function of the immature EEC filopodia and the molecular mechanisms that regulate the EEC filopodia formation require further investigation.

To investigate how gut microbiota regulate the EEC filopodia process and maturation, we generated GF and CV *Tg(neurod1:lifeActin-EGFP)* zebrafish. We imaged their proximal intestine at 7dpf. Our results demonstrated that about 15% of GF zebrafish EECs in the proximal intestine still have active filopodia actin filament at the base at 7dpf (Fig. 3E, G). The ratio of the EECs with active filopodia actin filament is significantly reduced in CV zebrafish (Fig. 3F, G). This data suggests that certain microbial cues promote EEC maturation and facilitate the disappearance of the EEC filopodia actin filament. This data is also consistent with the RNA seq results above, regarding the GF zebrafish EECs' increased gene expression associated with the actin-filament based process (Fig. 1G).

Previous mice studies suggested that EECs form an extended membrane process called "neuropod" to connect with the nervous system [3, 36]. Interestingly, we observed that some EECs in 7dpf zebrafish intestines formed an extended membrane process in the basal membrane that morphologically resembles the mammalian neuropod of EECs (Fig. S2C-D'). The extended membrane process is distinct from the thin actin filopodia filament and is not detected in 3dpf zebrafish EECs. The neuropod-like EECs are rare in the GF zebrafish intestine (Fig. S2A-B'). The CV zebrafish exhibit a significantly higher percentage of neuropod-like EECs in the intestine (Fig. S2E). Our data suggests the formation of the neuropod-like structures in mature EECs may require certain microbial cues.

Commensal microbiota promotes the formation of mitochondria hot spots in the EEC basal membrane.

Next, we seek to determine how gut microbiota regulate the EECs' mitochondria. We used a *Tg(neurod1:mitoEOS)* transgenic zebrafish model to visualize the EECs' mitochondria [37]. In this model, the green fluorescent EOS protein contains a mitochondrial tag that is expressed in EECs to label their mitochondria. Using this model, we can trace the EEC mitochondrial abundance and intracellular mitochondrial distribution in live zebrafish over time. Our results revealed that, from 3dpf to 5dpf, the zebrafish EEC did not significantly increase the mitochondrial abundance (Fig. S3A). However, at 6dpf, EECs exhibit higher mitochondrial abundance compared with 3dpf-5dpf EECs (Fig. S3A). Interestingly, at 3dpf, the mitochondria are evenly distributed within the EECs, and the mitochondrial contents near the basal lateral membrane are low (Fig. 4A-B', E). By 6dpf, most EECs exhibit hot spot mitochondrial distribution patterns (Fig. 4C-D', E). High mitochondrial contents are found at the base of EECs, presumably at the sites where EECs secrete vesicles (Fig. 4C-D', E). When we compare GF and CV zebrafish, commensal microbiota colonization did not increase the EEC mitochondrial abundance (Fig. S3B-C). However, the commensal microbiota colonization promotes the formation of mitochondrial hot spots at the basal membrane (Fig. 4F-H) and the CV zebrafish had higher mitochondrial contents near the basal membrane (Fig. 4F-G, I).

Mature EECs increase mitochondrial activity

To analyze the dynamic change of EECs' cellular and mitochondrial activity during their development and maturation process, we used the *Tg(neurod1:Gcamp6f); Tg(neurod1:mito-RGECO)* dual transgenic model [37]. In this model, the green

256 fluorescent calcium indicator protein Gcamp6f is expressed in the EEC cytoplasm. A red
257 fluorescent calcium indicator protein RGECO that contains a mitochondrial tag is
258 expressed in the EEC mitochondrial matrix. Therefore, by using this dual transgenic
259 model, we can simultaneously measure EEC cytoplasmic Ca^{2+} levels and mitochondrial
260 Ca^{2+} levels by measuring the change in green and red fluorescence (Video 4 and 5). We
261 then analyzed how EEC cytoplasmic and mitochondrial Ca^{2+} levels change during
262 development by tracing the same zebrafish from 3dpf to 6dpf (Fig. 5A-E''). Our results
263 showed that at 3dpf, the EECs exhibit low cytoplasmic and mitochondrial Ca^{2+} levels (Fig.
264 5B-B'', G, H). However, at 4dpf, there is a significant increase in both EEC cytoplasmic
265 and mitochondrial Ca^{2+} levels (Fig. 5C-C'', G, H). From 5dpf to 6dpf, the EEC cytoplasmic
266 Ca^{2+} levels decreased, while mitochondrial Ca^{2+} levels remained high (Fig. 5D-E'', G, H).
267 As a result, from 3dpf to 6dpf, the EEC mitochondrial to cytoplasmic Ca^{2+} ratio continues
268 to increase (Fig. 5F). A similar trend was found in all of the zebrafish samples that we
269 traced (Fig. 5I-K). When we grouped data of zebrafish of the same age together, we also
270 observed that as the EECs became more mature, the EECs increased their mitochondrial
271 to cytoplasmic Ca^{2+} level ratio (Fig. 5I-K).

272 **Gut microbiota increases resting EEC mitochondrial activity and spontaneous**
273 **firing**

274 Our new genetic zebrafish model and imaging approaches allow us to investigate how
275 gut microbiota changes EEC cytoplasmic and mitochondrial activity in vivo. We generated
276 *Tg(neurod1:Gcamp6f); Tg(neurod1:mitoRGECO)* GF and CV zebrafish and imaged the
277 fish's proximal intestinal EECs at 7dpf (Fig. 6A). First, we examined the absolute EEC
278 cellular plasma Ca^{2+} levels and EEC mitochondrial Ca^{2+} levels by analyzing the individual
279 EEC Gcamp6f and EEC mitoRGECO fluorescent levels in GF and CV zebrafish.
280 Compared to GF EECs, CV EECs exhibit significantly lower cytoplasmic and
281 mitochondrial Ca^{2+} levels (Fig. 6A-E). However, the CV EECs exhibit a significantly higher
282 mitochondrial to cytoplasmic Ca^{2+} ratio (Fig. 6A-D, F). Moreover, many of the EECs in the
283 CV but not GF zebrafish exhibit higher mitochondrial Ca2+ levels near the basal
284 membrane (Fig. 6C-D). These results suggest that gut microbiota may promote low
285 resting EEC cytoplasmic Ca^{2+} levels but enhance EEC mitochondrial activity. This finding
286 is consistent with the results from our RNA sequencing analysis above (Fig.2).

287 Using a 3D cell tracking approach, we can automatically track individual EECs and
288 analyze their Gcamp6f and mitoRGECO fluorescent change on a temporal scale. We
289 analyzed the relative EEC cytoplasmic Ca^{2+} and mitochondrial Ca^{2+} levels change in GF
290 and CV zebrafish. For each EEC, we normalized the EEC Gcamp6f, EEC mitoRGECO,
291 and EEC mitoRGECO/Gcamp6f ratio value to their values at time 0. Our results indicate
292 that some EECs in the CV zebrafish exhibit low amplitude firing as reflected by the
293 temporal fluctuation of the EEC cytoplasmic Ca^{2+} levels (Fig. 6K-M) (Video 6). However,
294 this spontaneous firing is not apparent in the GF zebrafish EECs (Fig. 6G-I) (Video 7).
295 Analysis of EECs across different GF and CV zebrafish samples indicate that ~21% of
296 CV EECs exhibit low amplitude firing, but only 2.5% of GF EECs exhibit low amplitude
297 firing (Fig. 6J, N). Those EECs with spontaneous firing increase the relative mitochondrial
298 Ca^{2+} levels but not the relative mitochondria-to-cytoplasm Ca^{2+} ratio (Fig. 6H, L). These

results suggest that at the resting condition, the CV EECs have higher mitochondrial activity, and their mitochondrial activity is more dynamic.

Nutrient-induced EEC mitochondrial calcium increase requires gut microbiota

As the primary sensory cells, one of the major functions of EECs is to sense the intestinal lumen's nutrients. Using the *Tg(neurod1:Gcamp6f)* zebrafish model, we previously developed a method to image live zebrafish's EEC response to nutrients using an epifluorescent microscope [24]. Our previous methods allowed us to examine the systemic intestinal EEC nutrient response. However, it does not enable us to image the EECs' nutrient sensing function at the cellular level [24]. To analyze how EECs respond to nutrients at the cellular level in live zebrafish, we developed a method to give stimulants to the zebrafish when we perform confocal imaging. Using 3D segmentation and 3D objective tracing, we can then quantify individual EECs' response to nutrient stimulation systemically (Fig. 7A). Similar to mammals, the zebrafish EECs respond to nutrient stimulants like fatty acid [24, 38]. Previous studies suggest that long-chain fatty acids like linoleic acid bind with the G-protein coupled receptor in zebrafish EECs, stimulating calcium release from ER (Fig. 7B) [38]. Whether nutrient stimulation modulates EEC mitochondrial Ca^{2+} levels remains unclear.

Using in vivo EEC calcium imaging and 3D automated cell tracing, we measured the individual EECs cytoplasmic and mitochondrial calcium response to nutrient stimulation systemically in live zebrafish (Fig. 7A) (video 8,9). Our results demonstrated that nutrients such as linoleic acid stimulate a subset of EECs and increase those EECs' cytoplasmic Ca^{2+} level (Fig. 7C-G) (Video 8, 9). Along with the EECs' cytoplasmic calcium increase, there is also a consistent mitochondrial calcium increase following nutrient stimulation (Fig. 7C-G) (Video 8, 9). In the linoleic acid-activated EECs, linoleic stimulation induces cytoplasmic calcium peak in these cells and the cellular cytoplasmic Ca^{2+} levels returned to their basal activity level (Fig. 7F-H). Their mitochondrial Ca^{2+} levels increased immediately following the cytoplasmic Ca^{2+} peak (Fig. 7F-H). However, unlike the cytoplasmic Ca^{2+}, the mitochondrial Ca^{2+} level remained higher than the basal Ca^{2+} level after the peak (Fig. 7F-H). As a result, the relative mitochondrial-to-cytoplasmic Ca^{2+} ratio increased post- linoleic acid stimulation (Fig. 7F-H). Moreover, our results demonstrate that the nutrient induced mitochondrial Ca^{2+} increase is more prominent in the mitochondria near the basal membrane (Fig. S4). This suggests that the nutrient induced mitochondrial Ca^{2+} increase is likely linked with the EECs' vesicle secretion process. Our results further indicate that the majority of the linoleic acid activated EECs in the conventionally raised zebrafish exhibit elevated mitochondrial calcium in response to nutrient stimulation (Fig. 7I-J).

Finally, we investigated whether and how gut microbiota regulates the EECs' nutrient response. We generated GF and CV *Tg(neurod1:Gcamp6f); Tg(neurod1:mitoRGECO)* zebrafish (Fig. 8A). We then stimulated the GF and CV zebrafish with linoleic acid and recorded how the GF and CV EECs responded to the linoleic stimulation. Our results indicate that, compared with CV zebrafish, the percentage of EECs that can be activated by linoleic acid in GF zebrafish is less (Fig. 8B). Within the activated EECs, the cytoplasmic Ca^{2+} amplitude remains the same between GF and CV groups (Fig. 8C).

342 However, within the activated EECs, the mitochondrial Ca^{2+} amplitude significantly
343 increased in the CV EECs (Fig. 8D, E-F). The same result is shown when we trace the
344 temporal EEC cytoplasmic and mitochondrial Ca^{2+} levels in GF and CV zebrafish (Fig.
345 8G-L). In most CV EECs, nutrient stimulation activates both cytoplasmic and
346 mitochondrial Ca^{2+} and increases the mitochondrial to cytoplasmic Ca^{2+} ratio (Fig. 8G).
347 However, the nutrient induced EEC mitochondrial activation is significantly reduced in GF
348 EECs (Fig. 8G-L). The nutrient induced mitochondrial-to-cytoplasmic Ca^{2+} ratio increase
349 is also impaired in GF EECs (Fig. 8I). These results suggest that the nutrient-induced
350 EEC mitochondrial activation requires signals from commensal microbiota colonization.

351 **Discussion**

352 In this study, by using transcriptomics, genetics, in vivo imaging, and gnotobiotic
353 manipulation, we revealed that commensal microbiota colonization is critical in shaping
354 EEC maturation and function during development (Fig. S5). Importantly, our data revealed
355 that commensal microbiota colonization is essential in promoting mitochondrial activity
356 and nutrient induced mitochondrial activation. Selectively manipulating gut microbial
357 signals to alter EEC mitochondrial function may open new opportunities to change EEC
358 vesicle secretion and EEC-neuronal communication.

359 **The change of EEC mitochondrial activity during development.**

360 Using in vivo imaging to track EECs during development in live zebrafish, our results
361 revealed that EEC mitochondrial activity is dynamically regulated during development.
362 Our data showed shortly after commensal microbiota colonization, EECs increase both
363 cytoplasmic and mitochondrial calcium activity. A phenomenon we referred to as the "EEC
364 awakening". After the EEC awakening, the EECs down-regulate their cytoplasmic calcium
365 levels but up-regulate their mitochondrial-to-cytoplasmic Ca^{2+} ratio. As sensory cells, it is
366 critical for EECs to maintain low cytoplasmic Ca^{2+} levels to enable a depolarization
367 potential. When EECs sense nutrient stimulants, the calcium ion channel on the cell
368 membrane or ER membrane will open [2]. Ca^{2+} from the extracellular space or the ER
369 lumen will flux into the cytoplasm matrix following the Ca^{2+} gradient. The low cytoplasmic
370 Ca^{2+} levels are, therefore, essential to generating the gradient to produce the Ca^{2+} peak
371 to trigger the downstream cellular signaling events [39]. Maintaining the membrane
372 potential or the low cytoplasmic Ca^{2+} levels consumes ATP [39]. ATP can be generated
373 via glycolysis or through the tricarboxylic acid cycle (TCA cycle) and oxidative
374 phosphorylation mediated by mitochondria [40]. It is well appreciated that mitochondrial
375 and metabolic remodeling is a central feature of differentiation and reprograming events
376 [17]. The mitochondrial oxidative metabolism is often suppressed in stem cells [41, 42].
377 The stem cells, including intestinal stem cells, rely on glycolysis to generate ATP [43, 44].
378 The mitochondria in stem cells remain functional [43]. However, stem cells possess
379 multiple mechanisms to suppress mitochondrial activity [44-46]. Upon differentiation,
380 mitochondrial activity increases [43, 44]. On the one hand, the increased mitochondrial
381 activity fuels the high metabolic demand of the differentiated cells. On the other hand, the
382 increased mitochondrial activity generates necessary signaling molecules such as
383 reactive oxygen species (ROS) and biosynthetic metabolites through the TCA cycle to
384 promote the differentiation process [47, 48]. The mitochondria-derived signaling

385 molecules also promote epigenetic remodeling and modulate gene expression [49]. Using
386 an *in vivo* EEC mitochondria imaging approach to trace the same zebrafish across
387 different developmental time points, our results revealed that the immature EECs at 3
388 days post fertilization display low mitochondrial activity. When zebrafish develop and
389 EECs start to be functional, mitochondrial activity increases. The increased mitochondrial
390 activity may not only provide energy to fuel the EEC cellular process but also provide the
391 signaling that is necessary for the EECs to mature and function. Interestingly, in addition
392 to the change in mitochondrial activity, we also observed changes in intracellular
393 mitochondrial distribution during development. Specifically, our results revealed the
394 increased mitochondrial contents at the basal lateral membrane during the EEC
395 maturation process. The increased mitochondrial distribution in the mature EECs is likely
396 to match the ATP demand of the vesicle secretion process in the basal lateral membrane.

397 In addition to providing energy, mitochondria also function as an important calcium buffer.
398 In response to extracellular stimulation, cytoplasmic Ca^{2+} levels increase. This increase
399 in cytoplasmic Ca^{2+} is quickly dissipated into intracellular organelles, such as the ER or
400 mitochondria. In most cells, mitochondrial calcium uptake is mediated by the
401 mitochondrial calcium uniporter (MCU), a calcium transporter protein in the mitochondrial
402 inner membrane. The electrochemical potential across the mitochondrial inner membrane,
403 generated by the respiration chain reaction, is the major driving force that enables calcium
404 influx into the mitochondrial matrix via MCU. Cytoplasmic and mitochondrial Ca^{2+} coupling
405 have not been studied in EECs. Our studies revealed that, in response to nutrient
406 stimulation, a subset of EECs increase cytoplasmic Ca^{2+} activity. Following the increase
407 of cytoplasmic Ca2+ levels, the mitochondrial Ca^{2+} levels increase in most activated EECs.
408 Though the cytoplasmic Ca^{2+} quickly returned to the basal level, most EEC mitochondrial
409 Ca^{2+} was continuously maintained at a high level. Basal mitochondrial respiratory function
410 might be the key to mediating Ca^{2+} flux into the mitochondrial matrix. The increase in
411 mitochondrial Ca^{2+} will increase mitochondrial respiration to sustain the ATP production
412 that is required for the EEC vesicle secretion in response to the nutrient stimulants [20].
413 Our results show that mitochondria are concentrated near the basal membrane, where
414 vesicle secretion occurs. Nutrient-induced mitochondrial activation is also most prominent
415 in the mitochondria near the base membrane. This evidence supports the hypothesis that
416 mitochondrial activation assists with vesicle secretion in mature EECs.

417 **The change of EEC morphology during development**

418 In addition to the change in EEC mitochondrial activity, another hallmark of EEC
419 maturation, revealed by our study, is the change in EEC morphology. Our study illustrated
420 for the first time that immature EECs possess dynamic and active actin filaments in the
421 basal membrane. However, the actin filaments disappeared in mature EECs. Instead,
422 some mature EECs formed an elongated basal lateral membrane process, a structure
423 that resembles the "neuropod" reported in previous mammalian studies [3]. Previous
424 studies demonstrated that the neuropod structure enriches the neurofilaments and
425 mitochondria [50]. EECs use neuropods to form synaptic connections with the underlying
426 nerve terminates, including the vagal sensory nerve [3, 4]. What regulates the EEC
427 neuropod formation and guides the EEC-neuronal synaptic connection remains unknown.
428 In developing neurons, neurites form actin-supported extensions known as growth cones

429 which seek synaptic targets [51]. Formation of the pre- and post-synaptic structures
430 disables the filipodium-enriched actin structure at the leading age [52]. Can the EECs
431 form a growth cone-like structure to find their targets and form synaptic connections with
432 the neurons? Our results revealed that the immature EECs form thin actin-based
433 elements in the basal lateral membrane, a structure that is similar to the filopodia
434 projections found in the developing neuron axon growth cone. In the zebrafish that are
435 colonized with commensal microbiota, these thin actin filaments in some of the EECs are
436 replaced by the "neuropod-like" structure when EECs mature. This morphology evidence
437 supported the hypothesis that the immature EECs may use active actin filaments to find
438 the synaptic targets and form the synaptic connections with the underlying neurons.
439 Establishing the EEC-neuronal connection will facilitate the EECs to transmit the ingested
440 nutrients to the nervous system.

441 **How does gut microbiota regulate EEC maturation and mitochondrial function?**

442 A major finding revealed by our study is that commensal microbiota colonization is critical
443 in supporting EEC maturation and promoting EEC mitochondrial function. Our results
444 established that microbiota colonization during early development might be critical in
445 establishing the organisms' appropriate nutrient-sensing function via promoting EEC
446 maturation. Our results also suggested that postnatal microbiota colonization might be
447 critical in promoting the formation of EEC-vagal neuronal communication as the
448 commensal microbiota colonization promotes the formation of the neuropod-like structure.
449 The EEC-vagal neuronal connection is essential in mediating gut-brain nutrient sensing.
450 Gut microbiota can therefore modulate EEC or EEC-vagal communication to regulate
451 brain nutrient perception and feeding behavior. Our results revealed that the EECs remain
452 in an immature state and exhibit low mitochondrial activity when commensal microbiota
453 is absent. Disrupting the commensal microbiota colonization or inhibiting the formation of
454 the healthy postnatal microbiome may produce devasting effects on gut nutrient
455 perception and metabolic regulation. The formation of the postnatal gut microbial
456 community is influenced by many factors (maternal microbiome, delivery method, milk-
457 feeding vs formula feeding). Previous research showed that disrupting the infant
458 microbiome through antibiotic exposure results in many side effects, including obesity and
459 weight gain later in life [53]. The EECs are critical in sensing ingested nutrients and
460 maintaining homeostasis [2]. Our study suggests that disrupting the commensal microbial
461 community early in life will change the EECs' function and maturity, which may change
462 how the body responds to ingested nutrients and affect energy homeostatic control.

463 The mitochondrial energetic adaptations encompass a conserved process that maintains
464 cell and organisms' fitness in the changing environment [54]. Our studies suggested that
465 in response to the commensal microbiota colonization, the EECs' increase mitochondrial
466 respiration and enhance the mitochondrial calcium activity. Our transcriptomic data
467 revealed that microbial induced EECs' energy and mitochondrial adaptation are involved
468 with the increased mitochondrial cristae formation and increased mitochondrial
469 respiratory chain assembly via enhancing mitochondrial protein import and facilitating
470 protein translation in the mitochondrial matrix (Fig. 2I). The EECs' mitochondrial energetic
471 adaptation in response to commensal microbiota colonization may contribute to the
472 systemic host adaptation to microbial colonization that is to compete to the limited

473 nutrients, enhance nutrient utilization efficiency and promote nutrient storage. The
474 microbial and molecular mechanisms by which microbial signals regulate mitochondrial
475 activity and intercede with the nutritional metabolism pathway within the EECs are
476 intriguing questions that require future investigations.

477 **Acknowledgments**

478 This work was supported by NIH K01-DK125527, The OSU Food for Health Research
479 Initiative Innovation Seed Grant, and The Global Probiotic Young Investigator Grant.

480 **Author contributions**

481 Alfahadh Alsudayri conducted the gnotobiotic experiments, some immunofluorescence
482 staining, and performed most of the data analysis. Shane Perelman performed the
483 experiments for EEC mitochondrial temporal tracking and data analysis. Annika Chura
484 performed some immunofluorescence staining experiments. Melissa Brewer and Maddie
485 McDevitt contributed to the data analysis and facilitated the experiments. Amrita Mandal
486 generated the *Tg(neurod1:mitoRGECO)* and the *Tg(neurod1:mitoEOS)* transgenic
487 zebrafish models. Dr. Catherine Drerup provided the *Tg(neurod1:mitoRGECO)* and the
488 *Tg(neurod1:mitoEOS)* transgenic zebrafish models and provided technique and
489 conceptual instructions. Lihua Ye directed the project and wrote the manuscript.

490 **Methods**

491 **Zebrafish strains and husbandry**

492 All zebrafish experiments conformed to the US Public Health Service Policy on Humane
493 Care and Use of Laboratory Animals, using protocol number 2021A00000091 approved
494 by the Institutional Animal Care and Use Committee of the Ohio State University.
495 Conventionally-reared adult zebrafish were reared and maintained on a recirculating
496 aquaculture system using established methods [28]. For experiments involving
497 conventionally-raised zebrafish larvae, adults were bred naturally in system water and
498 fertilized eggs were transferred to 100mm petri dishes containing ~25mL of egg water at
499 approximately 6 hours post-fertilization. The resulting larvae were raised under a 14h
500 light/10h dark cycle in an air incubator at 28°C at a density of 2 larvae/ml water. All the
501 experiments performed in this study ended at 7dpf unless specifically indicated. The
502 zebrafish lines used in this study are listed in Table 2. All lines were maintained on a EKW
503 background.

504 **Gnotobiotic zebrafish husbandry**

505 For experiments involving gnotobiotic zebrafish, we used our established methods to
506 generate germ-free zebrafish using natural breeding (ref.) with the following exception:
507 Gnotobiotic Zebrafish Medium (GZM) with antibiotics (AB-GZM) was supplemented with
508 50 µg/ml gentamycin (Sigma, G1264). Germ-free zebrafish eggs were maintained in cell
509 culture flasks with GZM at a density of 1 larvae/ml. From 3 dpf to 7 dpf, 60% daily media
510 change, and newborn fish food (Ultra Fresh Ltd.) feeding were performed as described
511 [28].

512 To generate conventionalized zebrafish, 15 mL filtered system water (5μm filter,
513 SLSV025LS, Millipore, final concentration of system water ~30%) was inoculated to flasks
514 containing germ-free zebrafish in GZM at 3 dpf when the zebrafish normally hatch from
515 their protective chorions. The same feeding and media change protocol was followed as
516 for germ free zebrafish. Microbial colonization density was determined via Colony
517 Forming Unit (CFU) analysis. To analyze the effect of high fat feeding on intestinal
518 bacteria colonization, dissected digestive tracts were dissected and pooled (5 guts/pool)
519 into 1mL sterile phosphate buffered saline (PBS) which was then mechanically
520 disassociated using a Tissue-Tearor (BioSpec Products, 985370). 100 μL of serially
521 diluted solution was then spotted on a Tryptic soy agar (TSA) plate and cultured overnight
522 at 30°C under aerobic conditions.

523 **Zebrafish EEC RNA sequencing analysis**

524 The zebrafish EEC RNA sequencing data was generated in our previous study (ref.). This
525 dataset can be accessed at GSE151711. Conventionalized (CV) and germ-free (GF)
526 *TgBAC(cldn15la:EGFP); Tg(neurod1:TagRFP)* ZM000 fed zebrafish larvae were derived
527 and reared using the published protocol [28] for Flow Activated Cell Sorting (FACS) to
528 isolate zebrafish EECs and other IECs. The protocol for FACS was adopted from a
529 previous publication [27]. Replicate pools of 50-100 double transgenic
530 *TgBAC(cldn15la:EGFP); Tg(neurod1:TagRPF)* zebrafish larvae were euthanized with
531 Tricaine and washed with deyolking buffer (55 mM NaCl, 1.8 mM KCl and 1.25 mM
532 NaHCO3) before they were transferred to dissociation buffer [HBSS supplemented with
533 5% heat-inactivated fetal bovine serum (HI-FBS, Sigma, F2442) and 10 mM HEPES
534 (Gibco, 15630–080)]. Larvae were dissociated using a combination of enzymatic
535 disruption using Liberase (Roche, 05 401 119 001, 5 μg/mL final), DNaseI (Sigma, D4513,
536 2 μg/mL final), Hyaluronidase (Sigma, H3506, 6 U/mL final) and Collagenase XI (Sigma,
537 C7657, 12.5 U/mL final) and mechanical disruption using a gentleMACS dissociator
538 (Miltenyi Biotec, 130-093-235). 400 μL of ice-cold 120 mM EDTA (in 1x PBS) wwas added
539 to each sample at the end of the dissociation process to stop the enzymatic digestion.
540 Following addition of 10 mL Buffer 2 [HBSS supplemented with 5% HI-FBS, 10 mM
541 HEPES and 2 mM EDTA], samples were filtered through 30 μm cell strainers (Miltenyi
542 Biotec, 130-098-458). Samples were then centrifuged at 1800 rcf for 15 minutes at room
543 temperature. The supernatant was decanted, and cell pellets were resuspended in 500
544 μL Buffer 2. FACS was performed with a MoFlo XDP cell sorter (Beckman Coulter) at the
545 Duke Cancer Institute Flow Cytometry Shared Resource. Single-color control samples
546 were used for compensation and gating. Viable EECs or IECs were identified as 7-AAD
547 negative.

548 Samples from three independent experimental replicates were performed. 250-580 EECs
549 (n=3 for each CV and GF group) and 100 IECs (n=3 for each CV and GF group) from
550 each experiment were used for library generation and RNA sequencing. Total RNA was
551 extracted from cell pellets using the Argencourt RNAdvance Cell V2 kit (Beckman)
552 following the manufacturer's instructions. RNA amplification prior to library preparation
553 had to be performed. The Clontech SMART-Seq v4 Ultra Low Input RNA Kit (Takara) was
554 used to generate full-length cDNA. mRNA transcripts were converted into cDNA through
555 Clontech's oligo(dT)-priming method. Full length cDNA was then converted into an

556 Illumina sequencing library using the Kapa Hyper Prep kit (Roche). In brief, cDNA was
557 sheared using a Covaris instrument to produce fragments of about 300 bp in length.
558 Illumina sequencing adapters were then ligated to both ends of the 300bp fragments prior
559 to final library amplification. Each library was uniquely indexed allowing for multiple
560 samples to be pooled and sequenced on two lanes of an Illumina HiSeq 4000 flow cell.
561 Each HiSeq 4000 lane could generate >330M 50bp single end reads per lane. This
562 pooling strategy generated enough sequencing depth (~55M reads per sample) for
563 estimating differential expression. Sample preparation and sequencing was performed at
564 the GCB Sequencing and Genomic Technologies Shared Resource.

565 Zebrafish RNA-seq reads were mapped to the danRer10 genome using HISAT2(Galaxy
566 Version 2.0.5.1) using default settings. Normalized counts and pairwise differentiation
567 analysis were carried out via DESeq2. The significance threshold of $p < 0.05$ was used
568 for comparison.

569 **Immunofluorescence staining**

570 Whole mount immunofluorescence staining was performed as previously described [24].
571 In brief, ice cold 2.5% formalin was used to fix zebrafish larvae overnight at 4°C. The
572 samples were then washed with PT solution (PBS+0.75%Triton-100). The skin and
573 remaining yolk were then removed using forceps under a dissecting microscope. The
574 deyolked samples were then permeabilized with methanol for more than 2 hrs at -20°C.
575 Samples were then blocked with 4% BSA at room temperature for more than 1 hr. The
576 primary antibody was diluted in PT solution and incubated at 4°C for more than 24 hrs.
577 Following primary antibody incubation, the samples were washed with PT solution and
578 incubated overnight with secondary antibody with Hoechst 33342 for DNA staining.
579 Imaging was performed with Nikon AXR confocal using the 20× of 40× water immersion
580 lens. The primary antibodies were listed in Table 1. The secondary antibodies in this
581 study were from Alexa Fluor Invitrogen were used at a dilution of 1:250.

582 **Live imaging and image analysis**

583 The zebrafish larvae were anesthetized with Tricaine methanesulfonate (MS222) and
584 were mounted in the 35mm confocal dish using 1% low-melting-Agar. All the in vivo
585 imaging were performed using the Nikon AXR confocal. When imaging the EEC cellular
586 and mitochondrial calcium activity using the *Tg(neurod1:Gcamp6f);*
587 *Tg(neurod1:mitoRGECO)* zebrafish, the zebrafish were not anesthetized due to the
588 effects of Tricaine in activating EECs. In the developmental tracing experiments, after
589 imaging, the zebrafish were dug out of the Agar, placed in 6-well plate, and returned to
590 the incubator until the next imaging time point. In the experiments when the temporal EEC
591 activity was traced, the images were collected using the resonate scanner. It takes less
592 than 10 seconds to collect the whole intestinal z-stack. The interval of time frames is 10
593 seconds. In the experiments when the nutrient stimulants were applied. A small window
594 was cut in front of the zebrafish, which allowed the zebrafish mouth to be exposed. First,
595 the zebrafish intestine was imaged before the stimulants were applied to assess the basal
596 line EEC activity. After collecting the baseline EEC activity, the image acquisition was
597 pulsed, and nutrient stimulants were added. The egg water in the confocal dish was

removed. 1ml nutrient stimulate solution was delivered into the window in front of the zebrafish. After the nutrient stimulation was applied, the image acquisition process resumes. The time lapse images were collected to assess the nutrient induced EEC activation. For the image analysis to assess the EEC calcium activity, the images were first aligned using the Nikon NLS element software. The threshold was defined using the Gcamp channel to perform segmentation of the individual EECs and identify individual EEC units. The non-EECs were filtered out via the shape criteria, the fluorescence intensity, and the size. The individual EEC units in different time frames were traced and tracked via the NLS element 3D-object tracing software. Due to the issues of gut motility, not every EEC in the zebrafish can be successfully traced throughout the time course. The mean fluorescence intensity of the individual EEC in each time frame will be calculated. The cluster 3.0 software was used to perform the clustering analysis of the EECs that exhibit different temporal calcium dynamics.

Main Figure Legends

Figure 1. Gut microbiota modulates the EEC subtype. (A) Gnotobiotic zebrafish experimental procedure to examine the effects of gut microbiota on EEC subtype formation. Commensal microbiota was colonized at 3pdf and the zebrafish were fixed at 7dpf for immunofluorescence staining. (B-C') Confocal projection of the representative germ-free (GF) and conventionalized (CV) zebrafish intestine. The total EECs were labeled by the *Tg(neurod1:EGFP)* transgene (green), and the PYY+EECs were labeled via the PYY antibody. (D-E') Confocal projection of the representative germ-free (GF) and conventionalized (CV) zebrafish intestine showing the ENK+ EECs. (F-G') Confocal projection of the representative germ-free (GF) and conventionalized (CV) zebrafish intestine showing the Trpa1+ EECs in the distal intestine. (H-I) Confocal projection of the representative germ-free (GF) and conventionalized (CV) zebrafish intestine showing the gcga+ EECs. (J-N) Quantification of the PYY+EECs, ENK+EECs, gcga+EECs, sst2+EECs and the Trpa1+EECs in GF and CV zebrafish. Student t-tests were used for statistical analysis. Each dot represents individual zebrafish. *$p<0.05$, *** $p<0.001$, **** $p<0.0001$.

Figure 2. Gut microbiota promotes EEC maturation and mitochondrial function. (A) Transcriptomic analysis of the FACS sorted EECs from GF and CV zebrafish. (B) Positive correlation between the genes that are upregulated in CV (X-axis) and the genes that are enriched in EECs (Y-axis). (C) Among the genes that are significantly upregulated in CV (red color), 74.5% are enriched in the EECs. (D) 72% of the EECs signature genes shared between zebrafish and mammals are upregulated in CV. (E) The differential expression of the EEC signature genes that encode hormone peptides or are involved in membrane potential in GF and CV conditions. * Indicates that the genes are significantly upregulated in the GF or CV conditions. (F) The volcano plot shows the genes that are significantly upregulated in CV or GF. (G) Go-term analysis of the CV or GF upregulated genes. (H) The volcano plot shows the genes that are involved in mitochondrial function. Many of the genes that are associated with mitochondrial regulation are among the most significantly

640 upregulated genes in CV EECs. (I) The model figure shows that commensal microbiota
641 colonization promotes EEC maturation and EEC mitochondrial function.

642 **Figure 3. EECs change morphology during development in a microbial-dependent**
643 **manner.** (A-B') Confocal projections of the proximal intestine *Tg(neurod1:lifeActin-EGFP)*
644 zebrafish at 3dpf and 6dpf in the fixed samples. The EECs in the 3 dpf but not 6 dpf
645 intestine exhibit thin actin filaments in the basal lateral membrane. (C-E') Live imaging
646 traces the same zebrafish's EECs at 3dpf and 6dpf. The EEC actin filaments are labeled
647 via the *Tg(neurod1:lifeActin-EGFP)*. (D-F') Zoom out view showing the typical 3dpf EEC
648 and 6dpf EEC. Note that at 3dpf, active actin filaments are observed at the basal lateral
649 membrane. At 6dpf, the actin filaments are only enriched in the apical brush border. (E-
650 F') Confocal projection of the 7 dpf GF and CV zebrafish EECs. The EEC actin filaments
651 are labeled via the *Tg(neurod1:lifeActin-EGFP)*. Note that the active basal lateral actin
652 filaments remained in a subpopulation of EECs in GF zebrafish. (G) Quantification of the
653 percentage of EECs with actin filaments in GF and CV conditions. Each dot represents
654 an individual zebrafish. Student-T test was used in G. *P<0.05.

655 **Figure 4. Commensal microbiota colonization promotes mitochondria**
656 **accumulation at the EEC basal lateral membrane.** (A-D') In vivo imaging to trace the
657 EEC mitochondrial abundance and the intracellular mitochondria distribution in the same
658 zebrafish. (A-B') Confocal projections of the typical EECs at 3dpf zebrafish proximal
659 intestine. (C-D') Confocal projections of the typical EECs at 6dpf zebrafish proximal
660 intestine. The mitochondria are labeled via the *Tg(neurod1:mitoEOS),* and the EECs are
661 labeled via the *Tg(neurod1:RFP)*. Note that at 3dpf, the mitochondria are evenly
662 distributed in the EEC cytoplasm, and the mitochondria contents at the basal lateral
663 membrane are low. At 6dpf, the mitochondria distribution exhibits a hot spot pattern. In
664 most EECs, a spot at the basal lateral membrane (yellow arrows in C-D') contains highly
665 abundant mitochondria. (E) Quantification of the relative mitochondrial fluorescence
666 intensity within the EECs in the same zebrafish at 3dpf and 6dpf. 5 representative EECs
667 from the same 3dpf and 6dpf zebrafish were used to perform the data analysis. (G-H')
668 Confocal projections of the typical EECs in GF and CV zebrafish. Note that many EECs
669 in GF zebrafish have low mitochondria contents at the basal lateral membrane (white
670 stars in G and G'). Most EECs in CV zebrafish exhibit hot spot basal lateral membrane
671 mitochondrial distribution patterns (yellow arrows in H and H'). (I) Quantification of the
672 percentage of EECs without basal mitochondrial hotspots in 7dpf GF and CV zebrafish.
673 Each dot represents an individual zebrafish. (I) Quantification of the mitochondrial
674 fluorescence intensity at the basal membrane in 7dpf GF and CV zebrafish. Student T-
675 test was used in H and I. * P<0.05, **** P<0.0001.

676 **Figure 5. The change of EEC mitochondrial activity during development.** (A) In vivo
677 imaging to trace the EEC cytoplasmic and mitochondrial calcium in the same zebrafish
678 from 3dpf to 6dpf. (B-E'') Confocal projections of the same *Tg(neurod1:Gcamp6f);*
679 *Tg(neurod1:mitoRGECO)* zebrafish at 3dpf, 4dpf, 5dpf, and 6dpf. The EEC cytoplasmic
680 Ca^{2+} level is represented via the Gcamp6f fluorescence (green). The EEC mitochondrial
681 Ca^{2+} level is displayed through mitoRGECO fluorescence (magenta). (F-H) Quantification
682 of the EEC mitochondria-to-cytoplasmic Ca^{2+} ratio, cytoplasmic Ca^{2+}, and mitochondrial
683 Ca^{2+} in the zebrafish represented in B-E''. (I-K) Combined quantification of 10 zebrafish

684 EECs mitochondria-to-cytoplasmic Ca^{2+} ratio, cytoplasmic Ca^{2+}, and mitochondrial Ca^{2+} .
685 Each dot in F-K represents an individual EEC. One-Way Anova followed by Tukey's post
686 test was used in F-K for statistical analysis. *p<0.05, ** p<0.01, *** p<0.001, **** p<0.0001.

687 **Figure 6. Commensal microbiota colonization alters the resting EEC cytoplasm and**
688 **mitochondria calcium activity.** (A) In vivo imaging to analyze the 7dpf GF and CV
689 zebrafish EEC cellular and mitochondrial activity. (B-C'') Confocal projection of the GF
690 and CV *Tg(neurod1:Gcamp6f); Tg(neurod1:mitoRGECO)* zebrafish. Note that the
691 absolute EEC Gcamp fluorescence is relatively higher in GF EECs. The EEC
692 mitoRGECO/Gcamp ratio is lower in GF EECs. The white arrows in B'' and C'' indicates
693 the EECs with higher mitochondrial activity near the base membrane. (C-D) zoom in view
694 shows representative EECs in GF (C) and CV (D) zebrafish mitochondrial calcium activity.
695 The CV EEC in D displayed high mitochondrial calcium near the base membrane (white
696 arrow). (D-F) Quantification of absolute Gcamp, mitoRGECO, and mitoRGECO/Gcamp
697 ratio in GF and CV zebrafish proximal intestinal EECs. Each dot represents an EEC. More
698 than five zebrafish were analyzed in each condition. (G-M) Analyze the relative EEC
699 Gcamp, EEC mitoRGECO, and EEC mitoRGECO/Gcamp ratio in GF and CV zebrafish
700 on a temporal scale. The EEC Gcamp, EEC mitoRGECO, and EEC mitoRGECO/Gcamp
701 ratio at each time point were normalized to t0. These quantification data sets reveal the
702 dynamic change of EEC cellular and mitochondrial activity in GF and CV conditions. Each
703 line in G-M represents an individual EEC. The red circles in G-M indicate the EECs that
704 exhibit Gcamp fluorescence fluctuation. These EECs that display dynamic Gcamp
705 fluorescence fluctuation were also referred to as active EECs in J and N. (J-N)
706 Quantification of the percentage of the quiet and active EECs in GF and CV zebrafish.
707 Student T-test was used in F for statistical analysis. * P<0.05, ** P<0.01.

708 **Figure 7. Analyze individual EEC cellular and mitochondrial activity in response to**
709 **nutrient stimulation in live zebrafish.** (A) Image and analyze the EEC cellular and
710 mitochondrial calcium activity before and after nutrient stimulation using the confocal
711 microscope. (B) The hypothesis model figure supported by our experimental data shows
712 fatty acid increases both cytoplasmic and mitochondrial Ca^{2+}. Long-chain fatty acids, such
713 as linoleic acid (LA), binds the fatty acid receptor at the cell membrane. Activating the
714 fatty acid receptor induces Ca^{2+} release from the ER and increases the cytoplasmic Ca^{2+}.
715 The increased cytoplasmic Ca^{2+} is then translocated into the mitochondrial matrix, which
716 increases the mitochondrial matrix's Ca^{2+} levels. The increased mitochondrial Ca^{2+}
717 promotes ATP production and powers EEC vesicle secretion. (C-E') Time-lapse images
718 of the whole zebrafish intestinal EECs' cytoplasmic and mitochondrial calcium change
719 post linoleic acid stimulation. The EEC cytoplasmic Ca^{2+} was labeled by Gcamp6f (green),
720 and the EEC mitochondrial Ca^{2+} was labeled by mitoRGECO (red). (F-G) Zoom-out view
721 shows two representative EECs that are activated by linoleic acid. (H) Analysis of
722 fluorescence change of Gcamp, mitoRGECO, and mitoRGECO/Gcamp ratio in a
723 presentative linoleic acid activated EEC. (I-J) Analysis of fluorescence change of Gcamp
724 and mitoRGECO of 68 EECs in one zebrafish before and after linoleic acid stimulation.
725 The EECs that increase cytoplasmic Ca^{2+} were defined as "LA activated EECs". Noted
726 that the majority of the linoleic activated EECs also exhibit increased mitochondrial
727 calcium.

728 **Figure 8. Nutrient induced EECs' mitochondrial calcium increase requires**
729 **commensal microbiota colonization.** (A) In vivo imaging to analyze the 7dpf GF and
730 CV zebrafish EEC cellular and mitochondrial activity in response to linoleic acid
731 stimulation. (B) Quantification of the percentage of EECs that are activated by linoleic
732 acid in GF and CV zebrafish. Each dot represents an individual zebrafish. (C-D)
733 Quantification of the linoleic acid-activated EEC cytoplasmic Ca^{2+} amplitudes and the
734 mitochondrial Ca^{2+} amplitudes in GF and CV zebrafish. Each dot represents an individual
735 EEC. Note that there is no significant change in the cytoplasmic Ca^{2+} increase. However,
736 CV EECs exhibit a significantly higher mitochondrial Ca^{2+} increase in response to linoleic
737 acid stimulation. (E-F) Time-lapse images of the representative EECs post linoleic acid
738 stimulation in GF and CV zebrafish. The EEC cytoplasmic Ca^{2+} was labeled by Gcamp6f,
739 and the EEC mitochondrial Ca^{2+} was labeled by mitoRGECO. (G-L) Analysis of the
740 change of the EEC Gcamp6f fluorescence, EEC mitoRGECO fluorescence, and EEC
741 mitoRGECO/Gcamp6f ratio in GF and CV zebrafish. Only the linoleic acid activated EECs
742 were plotted. G & J, H & K, and I & J used the same heatmap scale. 32 activated EECs
743 from 4 CV zebrafish and 50 activated EECs from 5 GF zebrafish were analyzed.

744

745 **Supplemental Figure Legends**

746 **Supplemental Figure 1. The EEC subtypes in zebrafish larvae**. (A) UMAP plots of the
747 zebrafish intestine single-cell RNA sequencing showing the zebrafish EECs and the five
748 EEC subtypes in zebrafish larvae. The zebrafish scRNA dataset is from Wen J. et al.,
749 2021. (B) The hormone profiles in the five zebrafish EEC subtypes. (C-E)
750 Immunofluorescence staining of the PYY+EEC subtype. Note that the PYY+EECs are
751 distributed in the proximal zebrafish intestine (C-C'). It overlaps with the secretory cell
752 marker 2F11 (D) but does not overlap with the marker for other EEC subtypes, such as
753 trpa1b (E). (F-K) Immunofluorescence staining of the Trpa1+EEC subtype. The single-
754 cell RNA seq data above demonstrate that the Trpa1+EECs (EEC5) express the peptide
755 enkephalin (ENK) and the enzyme that synthesizes serotonin (tph1b). (F-G)
756 Immunofluorescence staining of ENK confirms that only Trpa1+EECs express ENK (G).
757 Interestingly, ENK is only expressed in the Trpa1+EECs in the proximal intestine (F-F').
758 (H) Trpa1+EECs do not express sst2, a marker for the EEC subtype 1. (I-J) Tph1b is
759 expressed in the EECs. (K) Immunofluorescence staining showing part of the
760 Trpa1+EECs express 5-HT.

761 **Supplemental Figure 2. Commensal microbiota colonization promotes the**
762 **formation of "neuropod"-like structure in EECs.** (A-D') Confocal projections of the GF
763 and CV *Tg(neurod1:lifeActin-EGFP)* zebrafish. The yellow stars in A indicate EECs with
764 thin actin filaments at the basal lateral membrane. The White arrows in C and D indicate
765 the "neuropod" like elongated basal lateral membrane protrusions in CV EECs. (E)
766 Quantification of the EEC percentage that has "neuropod" like structure in GF and CV
767 conditions. Student T-test was used in E. Each dot represents an individual zebrafish. *
768 $P<0.05$.

Supplemental Figure 3. Gut microbiota did not alter the proximal intestine mitochondria abundance. (A) Quantification of the intracellular mitochondria abundance in the 3dpf to 6dpf zebrafish EECs. The mitochondrial abundance is represented by the *neurod1:mitoEOS* and *neurod1:RFP* fluorescence ratio in individual EECs. Each dot represents an EEC. 4 zebrafish were analyzed. (B-C) Quantification of the intracellular mitochondria abundance in the proximal and distal intestines of the GF and CV zebrafish. The mitochondrial abundance is represented by the *neurod1:mitoEOS* and *neurod1:RFP* fluorescence ratio in individual EECs. Each dot represents an EEC. More than 7 zebrafish in GF and CV groups were quantified. One-Way Anova followed by Tukey post-test was used in A. Student T-test was used in B and C. *** $P<0.001$, ** $P<0.01$.

Supplemental Figure 4. Nutrient stimulation prominently promotes mitochondrial Ca2+ to arise near the basal membrane. (A-B) Zoom in view shows two linoleic acid activated EECs in *Tg(neurod1:Gcamp6f); Tg(neurod1:mitoRGECO)* zebrafish. The cytoplasmic calcium was indicated with Gcamp6f (green fluorescence), and the mitochondrial calcium was indicated with mitoRGECO (magenta fluorescence). White arrows show activated mitochondria near the basal membrane.

Supplemental Figure 5. Model figure showing gut microbiota modulate EEC maturation and mitochondrial function. (A) During early development, the immature EECs exhibit low cytoplasmic Ca^{2+} and low mitochondrial Ca^{2+} levels. These immature EECs have active filapodial filaments at the basal lateral membrane. After the zebrafish hatched out and commensal microbiota started to colonize the zebrafish intestine, the EECs continued to develop and mature. Shortly after commensal microbiota colonization, the EECs increase both cytoplasmic and mitochondrial Ca^{2+} significantly ("EEC awakening"). After the EEC awakening, the EECs continue to mature and lose the basal lateral filapodial filaments. Some EECs form a neuropod. The mature EECs have low cytoplasmic Ca^{2+} but high mitochondria-to-cytoplasm Ca^{2+} ratio. (B) Commensal microbiota promotes EEC mitochondrial respiration function and increases mitochondrial inner membrane electronic potential ($\Delta\Psi m$). When nutrient stimulants, like fatty acids, stimulate the EECs, the EEC cytoplasmic Ca^{2+} rises. The high $\Delta\Psi m$ permits the cytoplasmic Ca^{2+} to flux into the mitochondrial matrix and power mitochondrial ATP production, which then promotes EEC vesicle release.

Supplemental Tables

Supplemental Table 1. The change of transcriptomics in GF and CV EECs.

Supplemental Table 2. The zebrafish lines and primary antibodies used in this manuscript.

Supplemental Videos

Supplemental Video 1. The 3dpf enterocytes do not have active filopodia filaments. The enterocyte actin was visualized via the *Tg(gata5:lifeActin-EGFP)* zebrafish line. The actin filaments were enriched in the brush border at the apical site.

Supplemental Video 2. The active EEC filopodia filaments in 3dpf EECs. The EEC filopodia at the EEC base is visualized via the *Tg(neurod1:lifeActin-EGFP)* zebrafish line.

Supplemental Video 3. The 6dpf EECs do not display active filopodia structure at the base. The majority of the 6dpf EECs displayed enriched actin filaments at the apical brush border.

Supplemental Video 4. Use the *Tg(neurod1:Gcamp6f); Tg(neurod1:mitoRGECO)* to simultaneously image the EECs' cytoplasmic and mitochondrial calcium.

Supplemental Video 5. The dynamic of the EEC mitochondrial calcium at the resting conditions in conventionally raised zebrafish.

Supplemental Video 6. The spontaneous calcium fluctuations in conventionalized (CV) zebrafish EECs. The EEC calcium dynamics were visualized using the *Tg(neurod1:Gcamp6f)* zebrafish.

Supplemental Video 7. The reduced calcium fluctuations in germ-free zebrafish EECs. The EEC calcium dynamics were visualized using the *Tg(neurod1:Gcamp6f)* zebrafish.

Supplemental Video 8. The Linoleic acid stimulation increases EEC cytoplasmic and mitochondrial calcium in conventionally raised zebrafish. The cytoplasmic calcium was visualized via the *Tg(neurod1:Gcamp6f)* (green) and the mitochondrial calcium was visualized via the *Tg(neurod1:mitoRGECO)* (magenta).

Supplemental Video 9. The Linoleic acid stimulation increases EEC mitochondrial calcium in conventionally raised zebrafish.

References

1. Duca, F.A., et al., *The metabolic impact of small intestinal nutrient sensing.* Nat Commun, 2021. **12**(1): p. 903.
2. Furness, J.B., et al., *The gut as a sensory organ.* Nat Rev Gastroenterol Hepatol, 2013. **10**(12): p. 729-40.
3. Bohorquez, D.V., et al., *Neuroepithelial circuit formed by innervation of sensory enteroendocrine cells.* J Clin Invest, 2015. **125**(2): p. 782-6.
4. Kaelberer, M.M., et al., *A gut-brain neural circuit for nutrient sensory transduction.* Science, 2018. **361**(6408).
5. Li, M., et al., *Gut-brain circuits for fat preference.* Nature, 2022. **610**(7933): p. 722-730.
6. Tan, H.E., et al., *The gut-brain axis mediates sugar preference.* Nature, 2020. **580**(7804): p. 511-516.
7. Buchanan, K.L., et al., *The preference for sugar over sweetener depends on a gut sensor cell.* Nat Neurosci, 2022. **25**(2): p. 191-200.

845 8. Ye, L. and J.F. Rawls, *Microbial influences on gut development and gut-brain*
846 *communication.* Development, 2021. **148**(21).
847 9. Yatsunenko, T., et al., *Human gut microbiome viewed across age and geography.* Nature,
848 2012. **486**(7402): p. 222-7.
849 10. Sprockett, D., T. Fukami, and D.A. Relman, *Role of priority effects in the early-life assembly*
850 *of the gut microbiota.* Nat Rev Gastroenterol Hepatol, 2018. **15**(4): p. 197-205.
851 11. Henning, S.J., *Postnatal development: coordination of feeding, digestion, and metabolism.*
852 Am J Physiol, 1981. **241**(3): p. G199-214.
853 12. Sommer, F. and F. Backhed, *The gut microbiota--masters of host development and*
854 *physiology.* Nat Rev Microbiol, 2013. **11**(4): p. 227-38.
855 13. Martinez-Guryn, K., et al., *Small Intestine Microbiota Regulate Host Digestive and*
856 *Absorptive Adaptive Responses to Dietary Lipids.* Cell Host Microbe, 2018. **23**(4): p. 458-
857 469 e5.
858 14. Semova, I., et al., *Microbiota regulate intestinal absorption and metabolism of fatty acids*
859 *in the zebrafish.* Cell Host Microbe, 2012. **12**(3): p. 277-88.
860 15. Yang, I., et al., *The Infant Microbiome: Implications for Infant Health and Neurocognitive*
861 *Development.* Nurs Res, 2016. **65**(1): p. 76-88.
862 16. Yu, K.B. and E.Y. Hsiao, *Roles for the gut microbiota in regulating neuronal feeding circuits.*
863 J Clin Invest, 2021. **131**(10).
864 17. Khacho, M. and R.S. Slack, *Mitochondrial activity in the regulation of stem cell self-renewal*
865 *and differentiation.* Curr Opin Cell Biol, 2017. **49**: p. 1-8.
866 18. Noguchi, M. and A. Kasahara, *Mitochondrial dynamics coordinate cell differentiation.*
867 Biochem Biophys Res Commun, 2018. **500**(1): p. 59-64.
868 19. Ludikhuize, M.C., et al., *Mitochondria Define Intestinal Stem Cell Differentiation*
869 *Downstream of a FOXO/Notch Axis.* Cell Metab, 2020. **32**(5): p. 889-900 e7.
870 20. Devine, M.J. and J.T. Kittler, *Mitochondria at the neuronal presynapse in health and disease.*
871 Nat Rev Neurosci, 2018. **19**(2): p. 63-80.
872 21. Kaufman, B.A., C. Li, and S.A. Soleimanpour, *Mitochondrial regulation of beta-cell function:*
873 *maintaining the momentum for insulin release.* Mol Aspects Med, 2015. **42**: p. 91-104.
874 22. Haythorne, E., et al., *Diabetes causes marked inhibition of mitochondrial metabolism in*
875 *pancreatic beta-cells.* Nat Commun, 2019. **10**(1): p. 2474.
876 23. Skibicka, K.P. and S.L. Dickson, *Enteroendocrine hormones - central effects on behavior.*
877 Curr Opin Pharmacol, 2013. **13**(6): p. 977-82.
878 24. Ye, L., et al., *High fat diet induces microbiota-dependent silencing of enteroendocrine cells.*
879 Elife, 2019. **8**.
880 25. Lavergne, A., et al., *Pancreatic and intestinal endocrine cells in zebrafish share common*
881 *transcriptomic signatures and regulatory programmes.* BMC Biol, 2020. **18**(1): p. 109.
882 26. Wen, J., et al., *Fxr signaling and microbial metabolism of bile salts in the zebrafish intestine.*
883 Sci Adv, 2021. **7**(30).
884 27. Ye, L., et al., *Enteroendocrine cells sense bacterial tryptophan catabolites to activate*
885 *enteric and vagal neuronal pathways.* Cell Host Microbe, 2021. **29**(2): p. 179-196 e9.
886 28. Melancon, E., et al., *Best practices for germ-free derivation and gnotobiotic zebrafish*
887 *husbandry.* Methods Cell Biol, 2017. **138**: p. 61-100.

29. Facer, P., et al., *Chromogranin: a newly recognized marker for endocrine cells of the human gastrointestinal tract.* Gastroenterology, 1985. **89**(6): p. 1366-73.
30. Taanman, J.W., *The mitochondrial genome: structure, transcription, translation and replication.* Biochim Biophys Acta, 1999. **1410**(2): p. 103-23.
31. Jourdain, A.A., et al., *The FASTK family of proteins: emerging regulators of mitochondrial RNA biology.* Nucleic Acids Res, 2017. **45**(19): p. 10941-10947.
32. Jourdain, A.A., et al., *A mitochondria-specific isoform of FASTK is present in mitochondrial RNA granules and regulates gene expression and function.* Cell Rep, 2015. **10**(7): p. 1110-21.
33. Sim, S.I., et al., *Structural basis of mitochondrial protein import by the TIM23 complex.* Nature, 2023.
34. Kondadi, A.K., R. Anand, and A.S. Reichert, *Cristae Membrane Dynamics - A Paradigm Change.* Trends Cell Biol, 2020. **30**(12): p. 923-936.
35. Mattila, P.K. and P. Lappalainen, *Filopodia: molecular architecture and cellular functions.* Nat Rev Mol Cell Biol, 2008. **9**(6): p. 446-54.
36. Reinshagen, M., *[A gut-brain neural circuit for nutrient sensory transduction].* Z Gastroenterol, 2019. **57**(3): p. 335.
37. Mandal, A., K. Pinter, and C.M. Drerup, *Analyzing Neuronal Mitochondria in vivo Using Fluorescent Reporters in Zebrafish.* Front Cell Dev Biol, 2018. **6**: p. 144.
38. Lu, V.B., F.M. Gribble, and F. Reimann, *Free Fatty Acid Receptors in Enteroendocrine Cells.* Endocrinology, 2018. **159**(7): p. 2826-2835.
39. Berridge, M.J., M.D. Bootman, and H.L. Roderick, *Calcium signalling: dynamics, homeostasis and remodelling.* Nat Rev Mol Cell Biol, 2003. **4**(7): p. 517-29.
40. Bonora, M., et al., *ATP synthesis and storage.* Purinergic Signal, 2012. **8**(3): p. 343-57.
41. Prigione, A., et al., *The senescence-related mitochondrial/oxidative stress pathway is repressed in human induced pluripotent stem cells.* Stem Cells, 2010. **28**(4): p. 721-33.
42. Cho, Y.M., et al., *Dynamic changes in mitochondrial biogenesis and antioxidant enzymes during the spontaneous differentiation of human embryonic stem cells.* Biochem Biophys Res Commun, 2006. **348**(4): p. 1472-8.
43. Folmes, C.D., et al., *Somatic oxidative bioenergetics transitions into pluripotency-dependent glycolysis to facilitate nuclear reprogramming.* Cell Metab, 2011. **14**(2): p. 264-71.
44. Schell, J.C., et al., *Control of intestinal stem cell function and proliferation by mitochondrial pyruvate metabolism.* Nat Cell Biol, 2017. **19**(9): p. 1027-1036.
45. Zhang, J., et al., *UCP2 regulates energy metabolism and differentiation potential of human pluripotent stem cells.* EMBO J, 2016. **35**(8): p. 899.
46. Sanchez-Arago, M., et al., *Degradation of IF1 controls energy metabolism during osteogenic differentiation of stem cells.* EMBO Rep, 2013. **14**(7): p. 638-44.
47. Khacho, M., et al., *Mitochondrial Dynamics Impacts Stem Cell Identity and Fate Decisions by Regulating a Nuclear Transcriptional Program.* Cell Stem Cell, 2016. **19**(2): p. 232-247.
48. Wellen, K.E., et al., *ATP-citrate lyase links cellular metabolism to histone acetylation.* Science, 2009. **324**(5930): p. 1076-80.
49. Kaelin, W.G., Jr. and S.L. McKnight, *Influence of metabolism on epigenetics and disease.* Cell, 2013. **153**(1): p. 56-69.

932 50. Bohorquez, D.V., et al., *An enteroendocrine cell-enteric glia connection revealed by 3D*
933 *electron microscopy.* PLoS One, 2014. **9**(2): p. e89881.
934 51. Tamariz, E. and A. Varela-Echavarria, *The discovery of the growth cone and its influence on*
935 *the study of axon guidance.* Front Neuroanat, 2015. **9**: p. 51.
936 52. Dent, E.W., S.L. Gupton, and F.B. Gertler, *The growth cone cytoskeleton in axon outgrowth*
937 *and guidance.* Cold Spring Harb Perspect Biol, 2011. **3**(3).
938 53. Aversa, Z., et al., *Association of Infant Antibiotic Exposure With Childhood Health*
939 *Outcomes.* Mayo Clin Proc, 2021. **96**(1): p. 66-77.
940 54. Bennett, C.F., P. Latorre-Muro, and P. Puigserver, *Mechanisms of mitochondrial respiratory*
941 *adaptation.* Nat Rev Mol Cell Biol, 2022. **23**(12): p. 817-835.
942

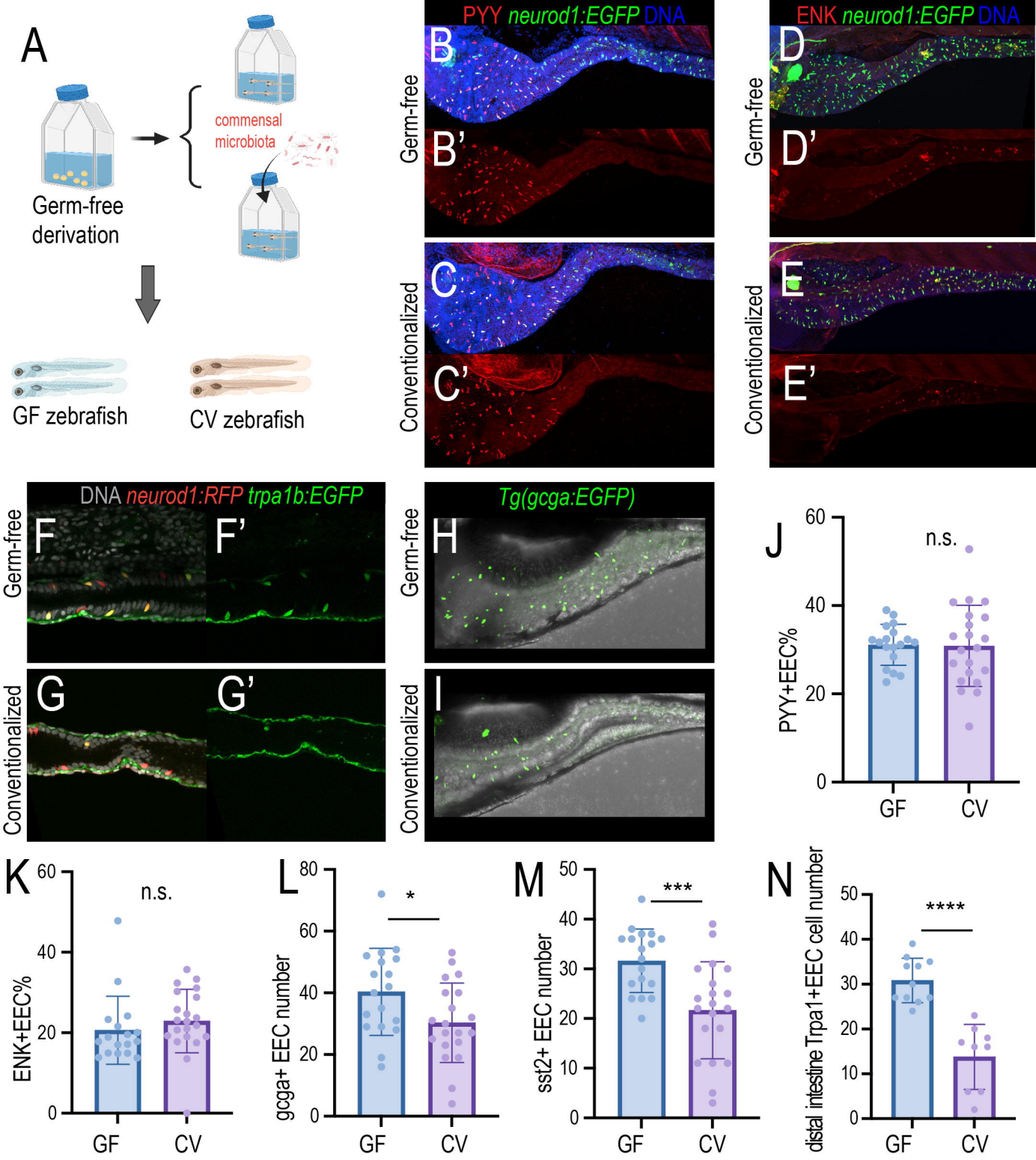
A
Germ-free derivation
commensal microbiota
GF zebrafish
CV zebrafish
PYY neurod1:EGFP DNA
ENK neurod1:EGFP DNA
Germ-free
Conventionalized
B
B'
C
C'
D
D'
E
E'
DNA neurod1:RFP trpa1b:EGFP
F
F'
G
G'
Tg(gcga:EGFP)
H
I
J
PYY+EEC%
n.s.
K
ENK+EEC%
n.s.
L
gcga+ EEC number
*
M
sst2+ EEC number
***
N
distal intestine Trpa1+EEC cell number
****
GF
CV

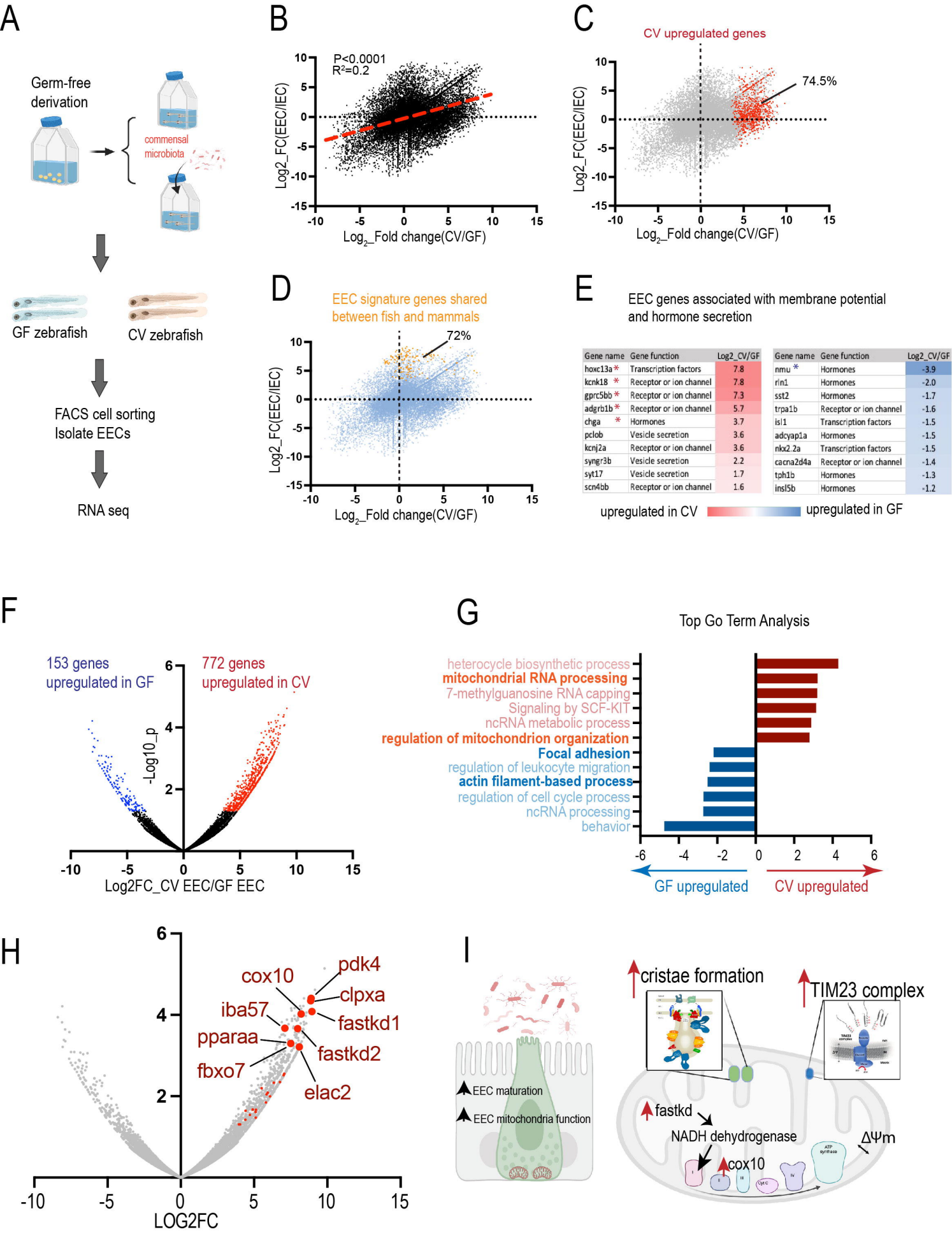
A
Germ-free derivation
commensal microbiota
GF zebrafish
CV zebrafish
FACS cell sorting
Isolate EECs
RNA seq
B
P<0.0001
R²=0.2
Log2_FC(EEC/IEC)
Log2_Fold change(CV/GF)
C
CV upregulated genes
74.5%
Log2_FC(EEC/IEC)
Log2_Fold change(CV/GF)
D
EEC signature genes shared between fish and mammals
72%
Log2_FC(EEC/IEC)
Log2_Fold change(CV/GF)
E
EEC genes associated with membrane potential and hormone secretion
upregulated in CV
upregulated in GF
F
153 genes upregulated in GF
772 genes upregulated in CV
-Log10_p
Log2FC_CV EEC/GF EEC
G
Top Go Term Analysis
heterocycle biosynthetic process
mitochondrial RNA processing
7-methylguanosine RNA capping
Signaling by SCF-KIT
ncRNA metabolic process
regulation of mitochondrion organization
Focal adhesion
regulation of leukocyte migration
actin filament-based process
regulation of cell cycle process
ncRNA processing
behavior
GF upregulated
CV upregulated
H
cox10
pdk4
clpxa
iba57
fastkd1
pparaa
fastkd2
fbxo7
elac2
LOG2FC
I
EEC maturation
EEC mitochondria function
cristae formation
TIM23 complex
fastkd
NADH dehydrogenase
cox10
ΔΨm

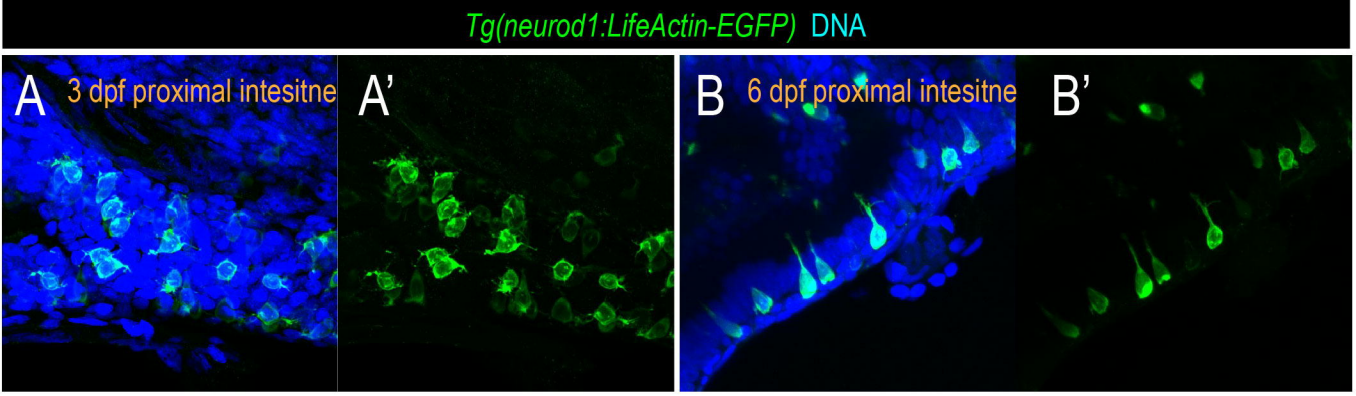
Tg(neurod1:LifeActin-EGFP) DNA
A
3 dpf proximal intesitne
A'
B
6 dpf proximal intesitne
B'

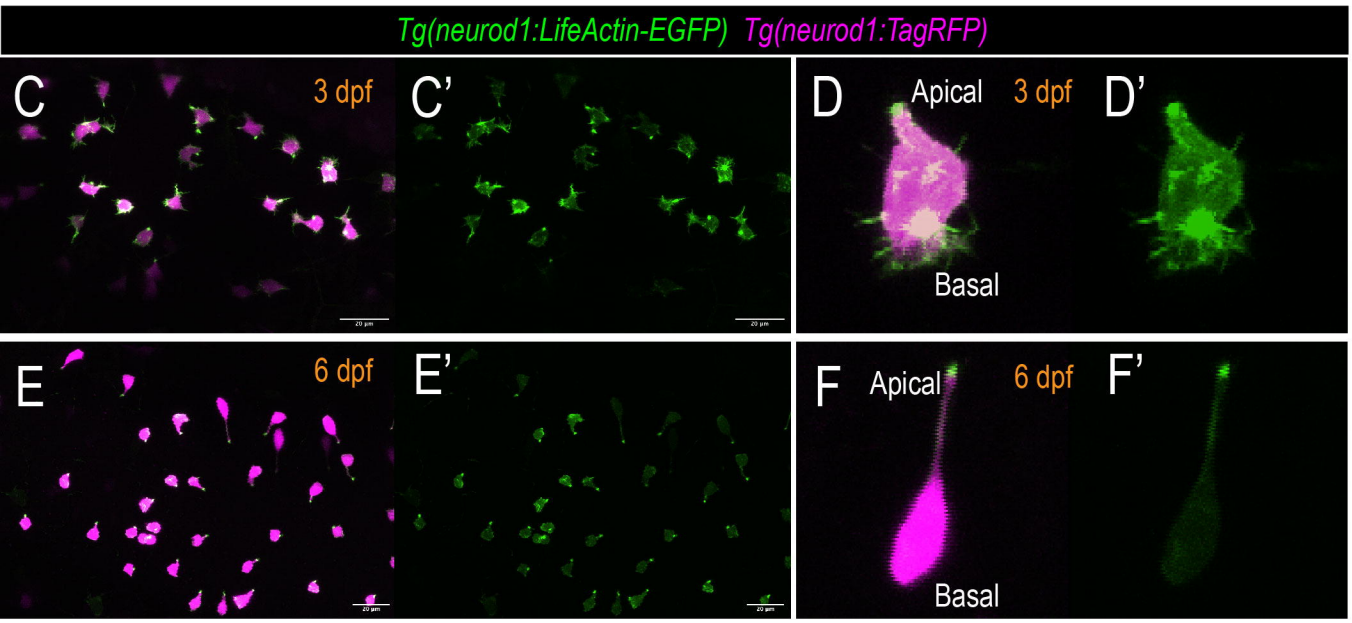
Tg(neurod1:LifeActin-EGFP) Tg(neurod1:TagRFP)
C
3 dpf
C'
D
Apical
3 dpf
D'
Basal
E
6 dpf
E'
F
Apical
6 dpf
F'
Basal

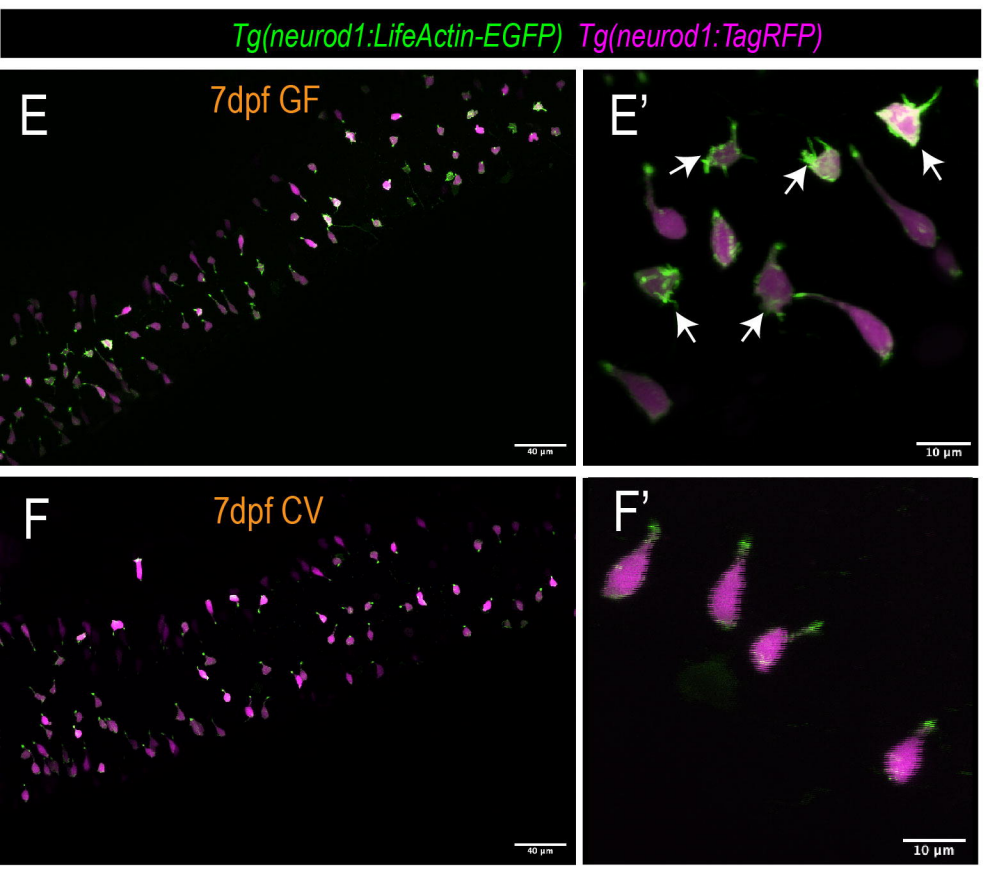
Tg(neurod1:LifeActin-EGFP) Tg(neurod1:TagRFP)
E
7dpf GF
40 µm
E'
10 µm
F
7dpf CV
40 µm
F'
10 µm

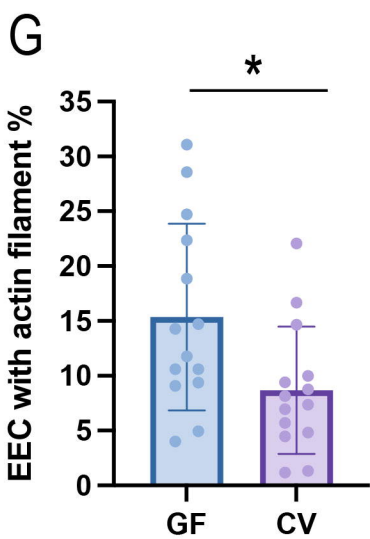
G
*
EEC with actin filament %
35
30
25
20
15
10
5
0
GF
CV

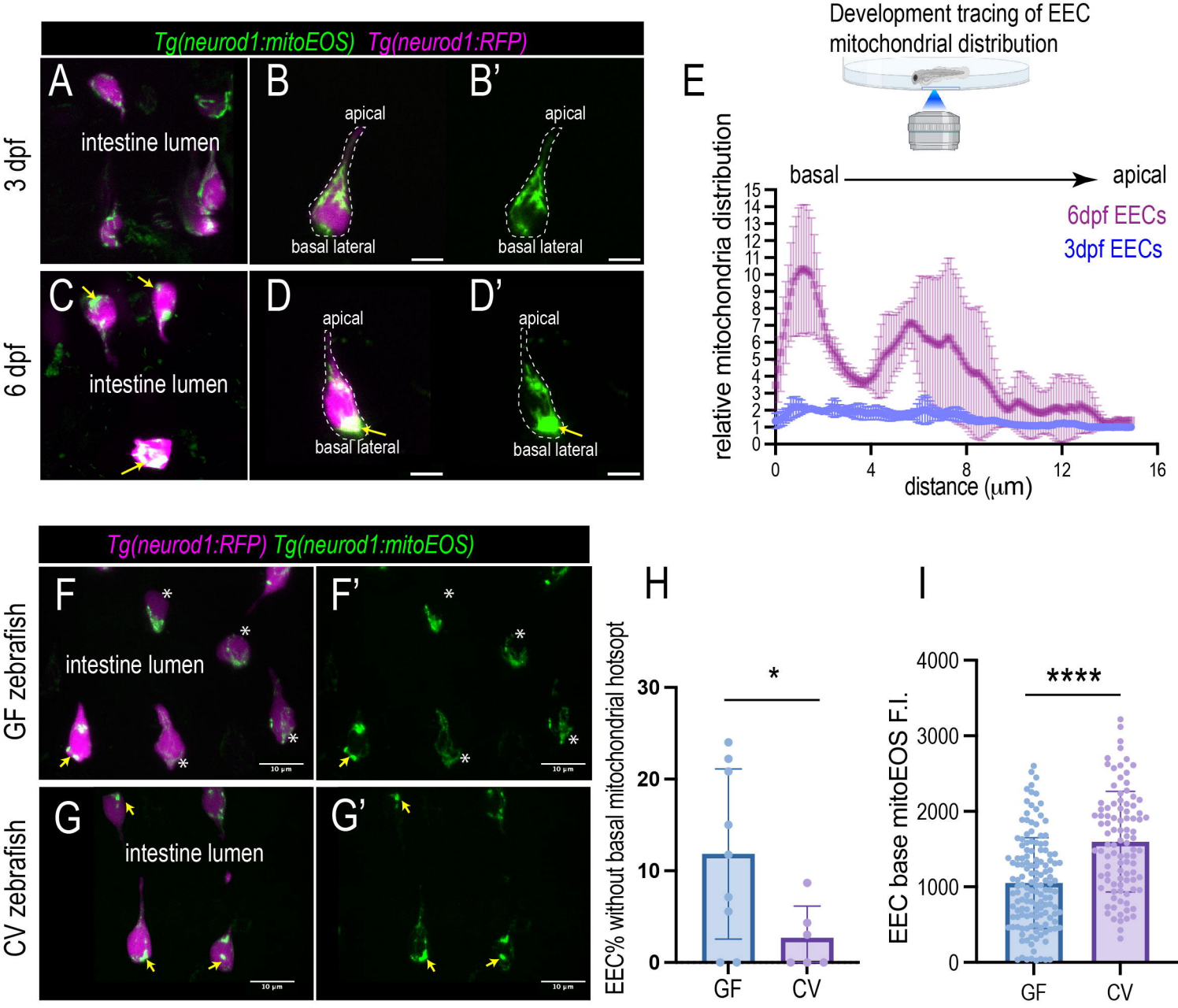
Tg(neurod1:mitoEOS) Tg(neurod1:RFP)
A
B
B'
C
D
D'
3 dpf
6 dpf
intestine lumen
apical
basal lateral
Development tracing of EEC mitochondrial distribution
E
basal
apical
6dpf EECs
3dpf EECs
relative mitochondria distribution
distance (μm)
Tg(neurod1:RFP) Tg(neurod1:mitoEOS)
F
F'
G
G'
GF zebrafish
CV zebrafish
10 μm
H
I
EEC% without basal mitochondrial hotspot
EEC base mitoEOS F.I.
GF
CV

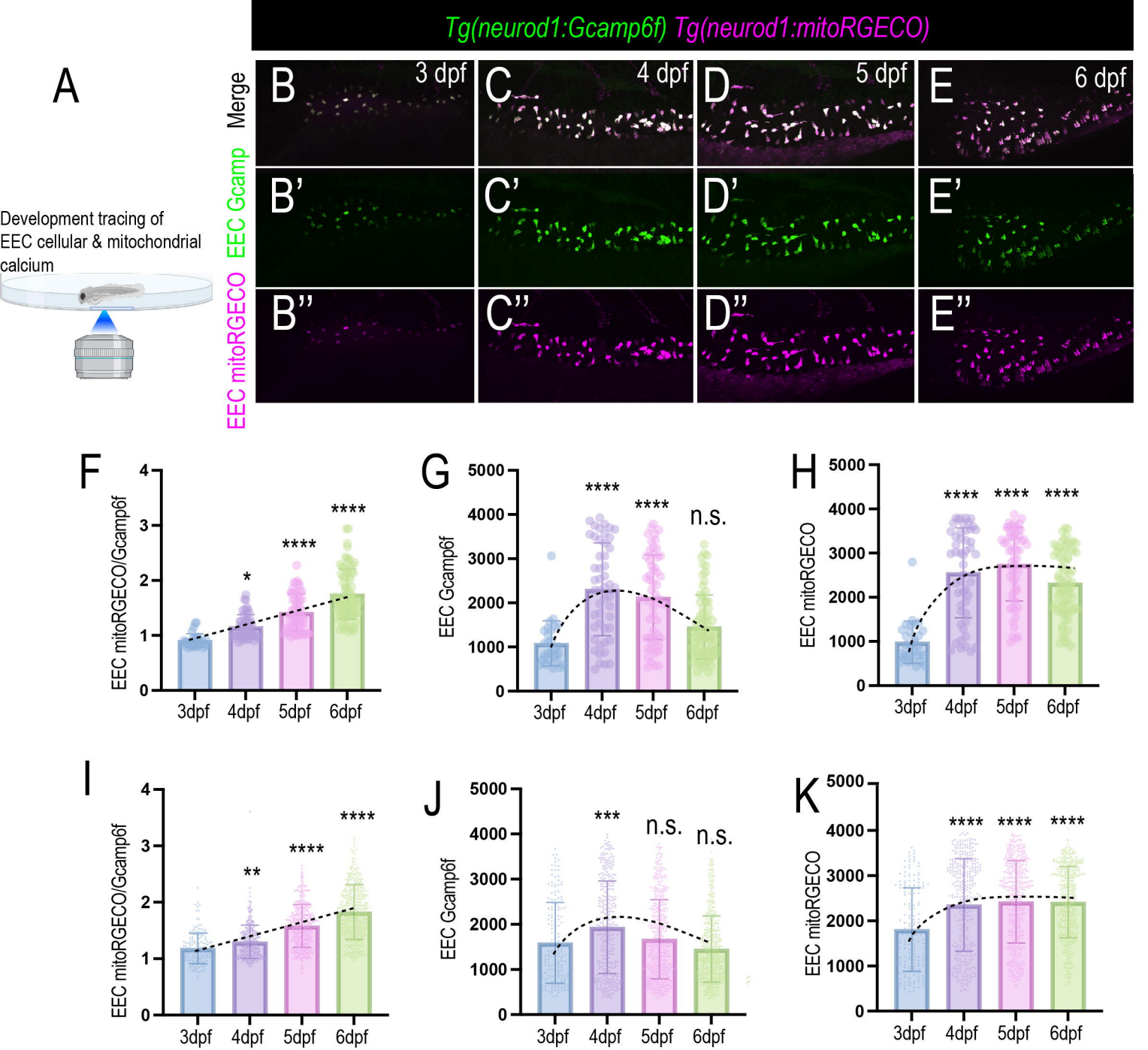
Tg(neurod1:Gcamp6f) Tg(neurod1:mitoRGECO)
A
Development tracing of EEC cellular & mitochondrial calcium
Merge
EEC Gcamp
EEC mitoRGECO
B 3 dpf
C 4 dpf
D 5 dpf
E 6 dpf
B'
C'
D'
E'
B''
C''
D''
E''
F
EEC mitoRGECO/Gcamp6f
3dpf 4dpf 5dpf 6dpf
G
EEC Gcamp6f
n.s.
H
EEC mitoRGECO
I
EEC mitoRGECO/Gcamp6f
J
EEC Gcamp6f
n.s.
K
EEC mitoRGECO

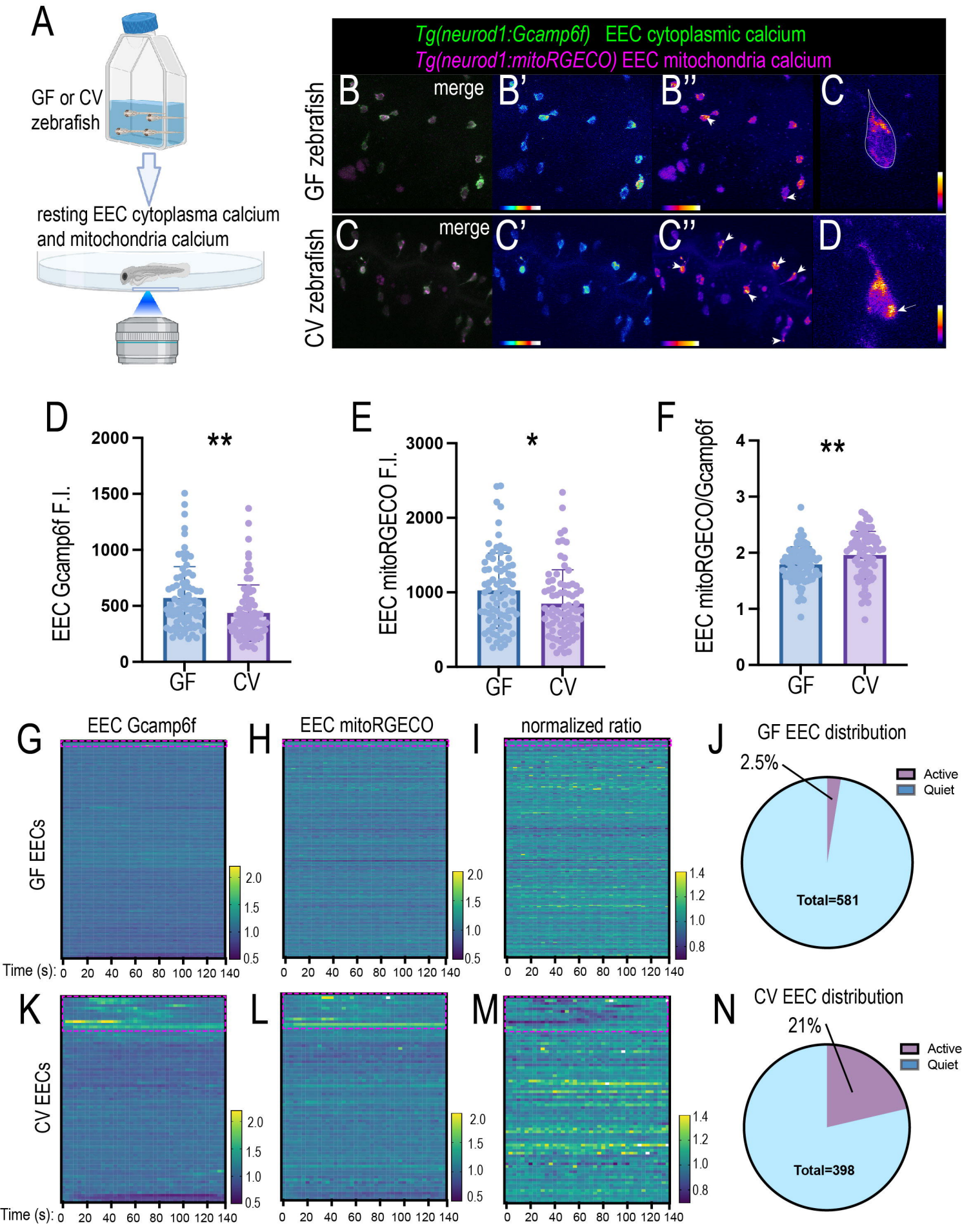
A
GF or CV zebrafish
resting EEC cytoplasma calcium and mitochondria calcium
Tg(neurod1:Gcamp6f) EEC cytoplasmic calcium
Tg(neurod1:mitoRGECO) EEC mitochondria calcium
GF zebrafish
CV zebrafish
B
merge
B'
B''
C
C
merge
C'
C''
D
D
EEC Gcamp6f F.I.
**
GF
CV
E
EEC mitoRGECO F.I.
*
F
EEC mitoRGECO/Gcamp6f
**
G
EEC Gcamp6f
H
EEC mitoRGECO
I
normalized ratio
GF EECs
Time (s):
J
GF EEC distribution
2.5%
Active
Quiet
Total=581
K
L
M
CV EECs
N
CV EEC distribution
21%
Total=398

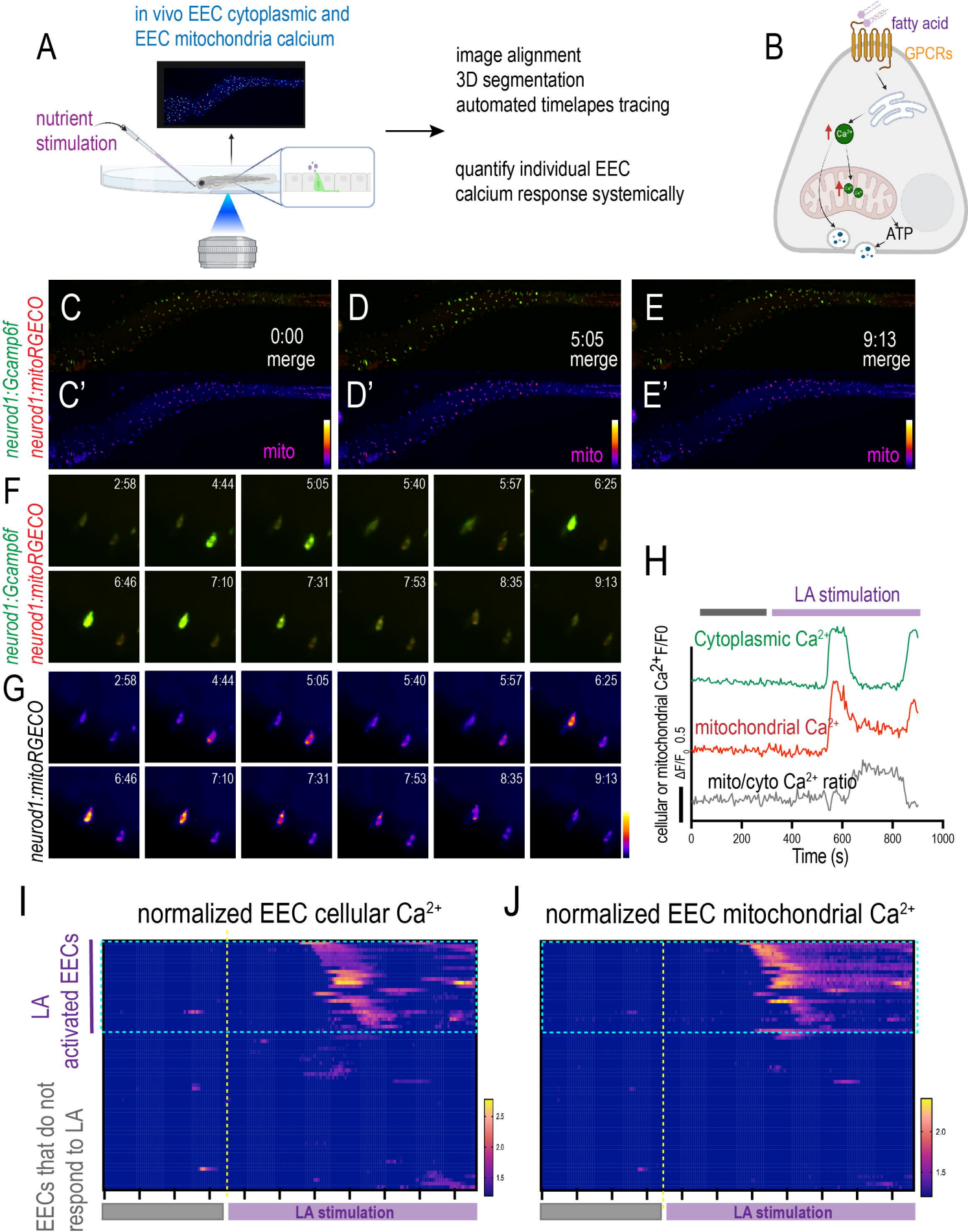
A
in vivo EEC cytoplasmic and
EEC mitochondria calcium
nutrient
stimulation
image alignment
3D segmentation
automated timelapes tracing
quantify individual EEC
calcium response systemically
B
fatty acid
GPCRs
ATP
C
0:00
merge
C'
mito
D
5:05
merge
D'
mito
E
9:13
merge
E'
mito
neurod1:Gcamp6f
neurod1:mitoRGECO
F
2:58
4:44
5:05
5:40
5:57
6:25
6:46
7:10
7:31
7:53
8:35
9:13
G
neurod1:mitoRGECO
H
LA stimulation
Cytoplasmic Ca2+
mitochondrial Ca2+
mito/cyto Ca2+ ratio
cellular or mitochondrial Ca2+F/F0
ΔF/F0 0.5
0
200
400
600
800
1000
Time (s)
I
normalized EEC cellular Ca2+
LA
activated EECs
EECs that do not
respond to LA
2.5
2.0
1.5
LA stimulation
J
normalized EEC mitochondrial Ca2+
2.0
1.5
LA stimulation

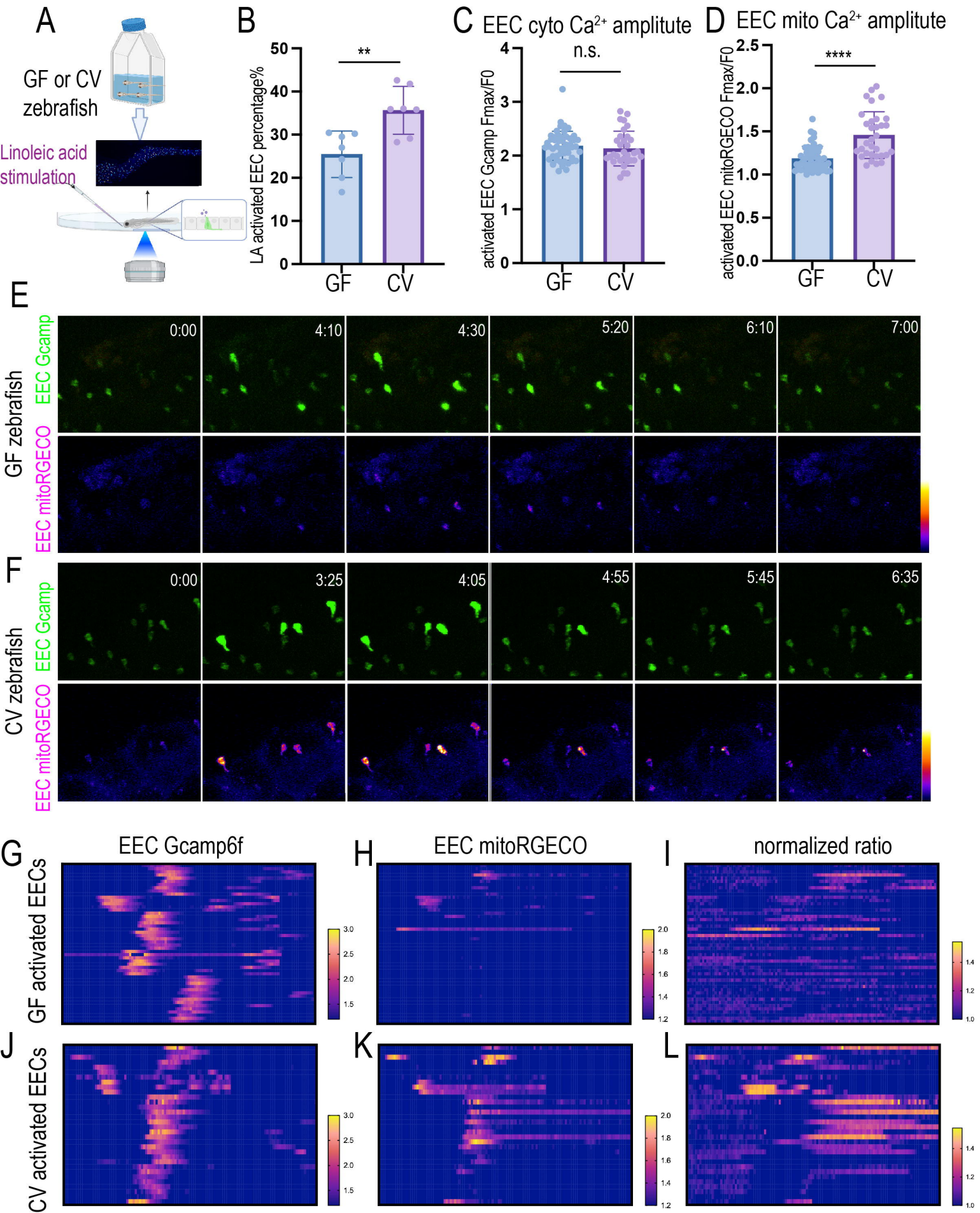
A
GF or CV zebrafish
Linoleic acid stimulation
B
LA activated EEC percentage%
**
GF
CV
C
EEC cyto Ca2+ amplitute
activated EEC Gcamp Fmax/F0
n.s.
GF
CV
D
EEC mito Ca2+ amplitute
activated EEC mitoRGECO Fmax/F0
****
GF
CV
E
GF zebrafish
EEC Gcamp
EEC mitoRGECO
0:00
4:10
4:30
5:20
6:10
7:00
F
CV zebrafish
EEC Gcamp
EEC mitoRGECO
0:00
3:25
4:05
4:55
5:45
6:35
G
EEC Gcamp6f
GF activated EECs
H
EEC mitoRGECO
I
normalized ratio
J
CV activated EECs
K
L

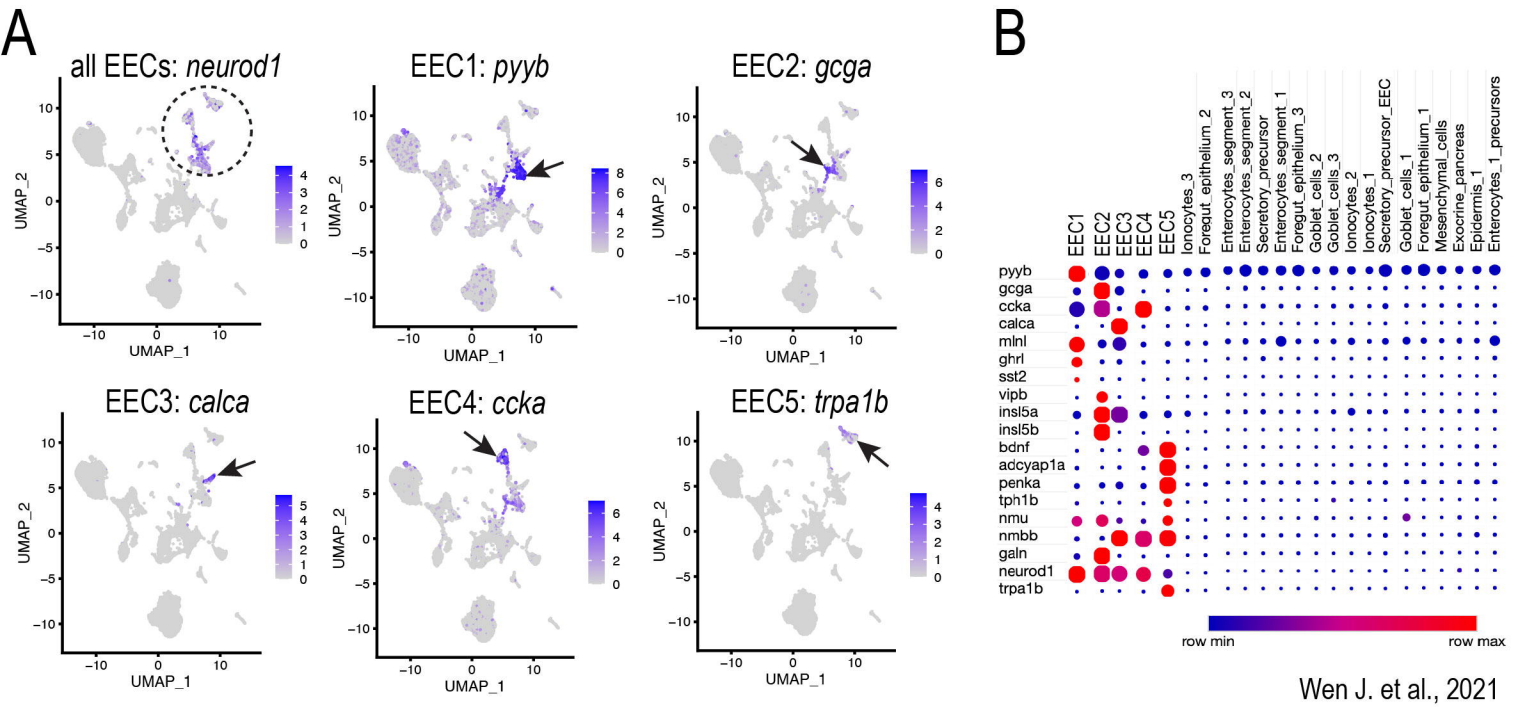

Wen J. et al., 2021

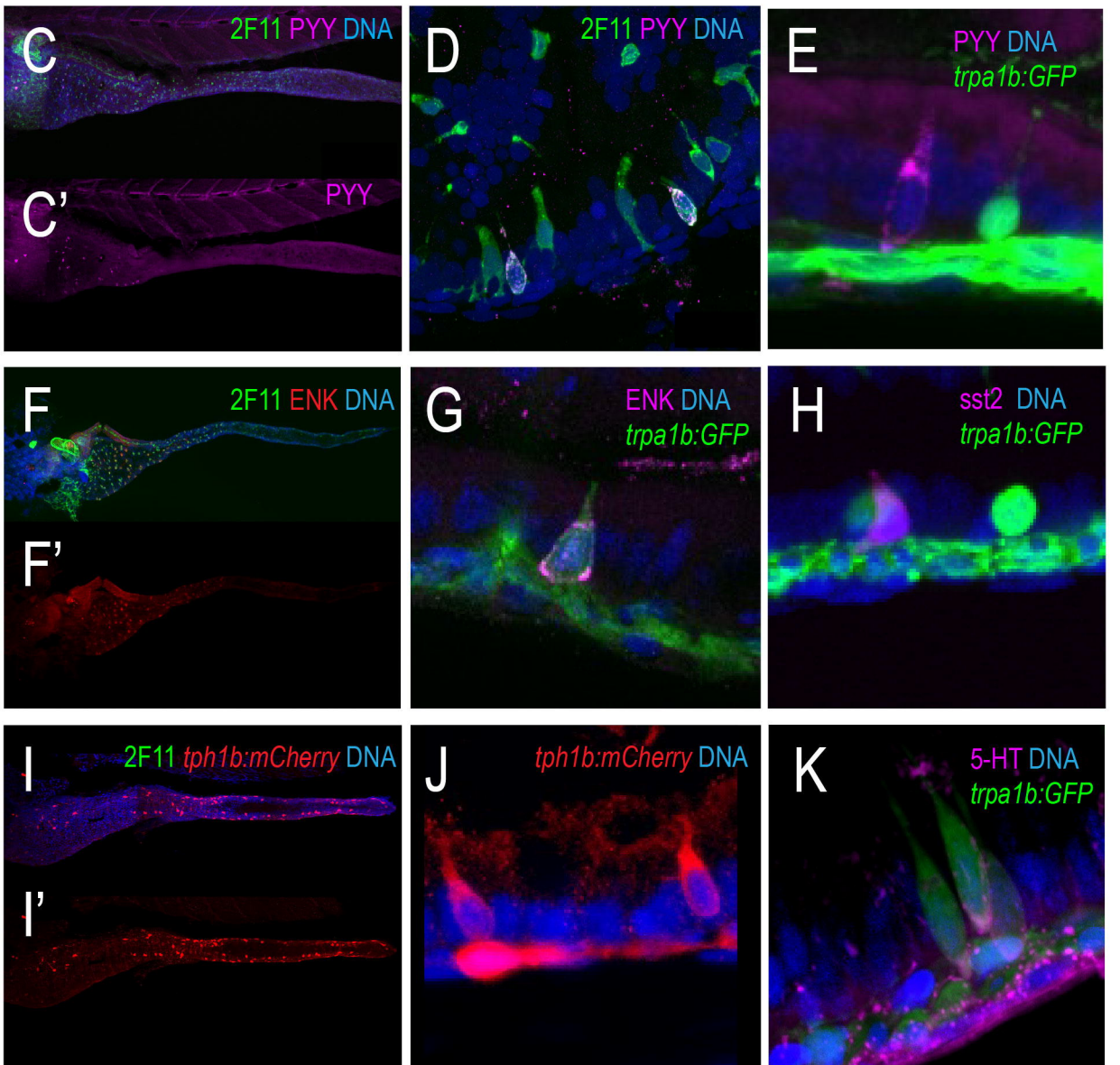

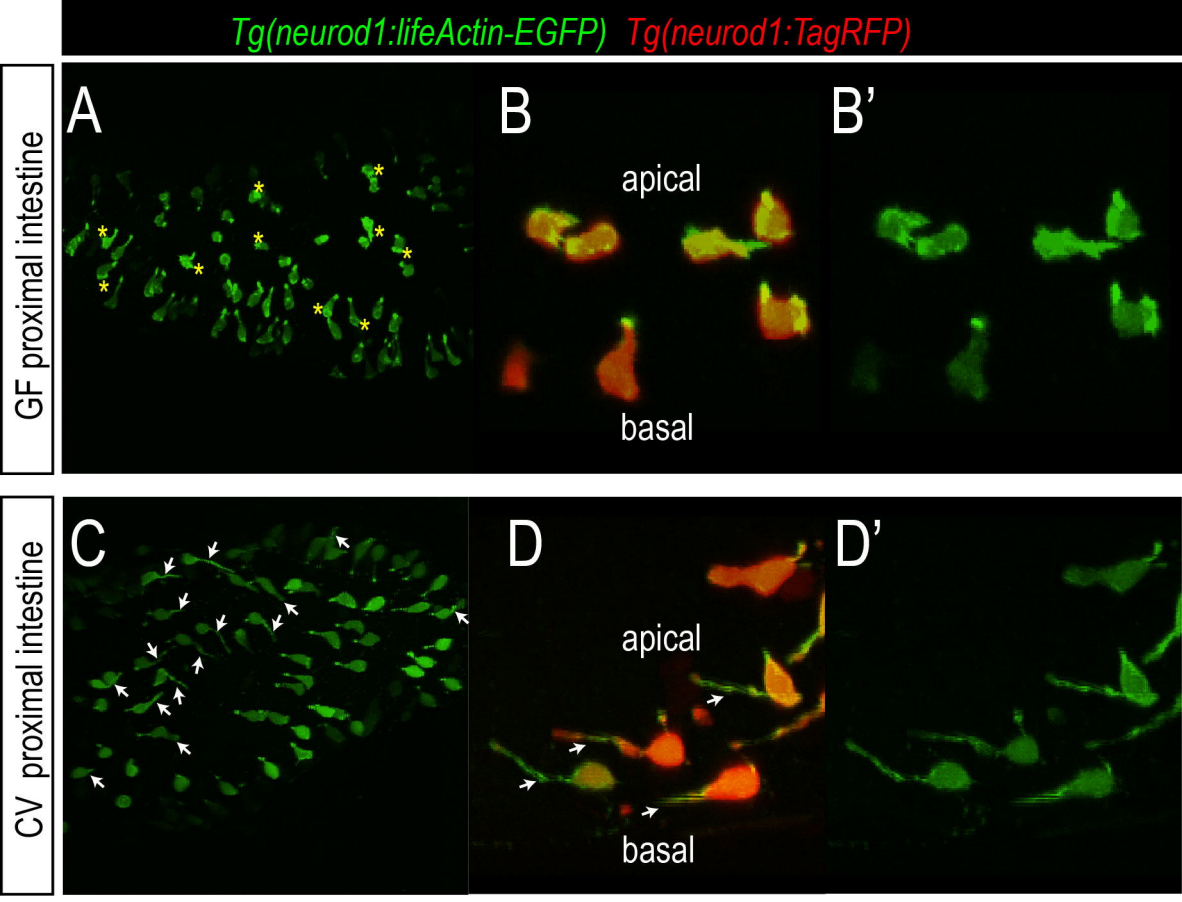
Tg(neurod1:lifeActin-EGFP) Tg(neurod1:TagRFP)
GF proximal intestine
CV proximal intestine
A
B
B'
C
D
D'
apical
basal
apical
basal

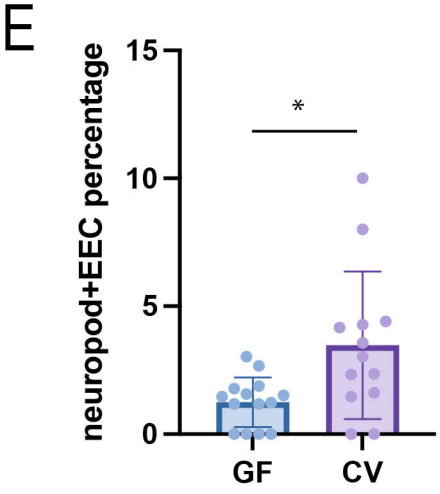
E
neuropod+EEC percentage
15
10
5
0
*
GF
CV

A

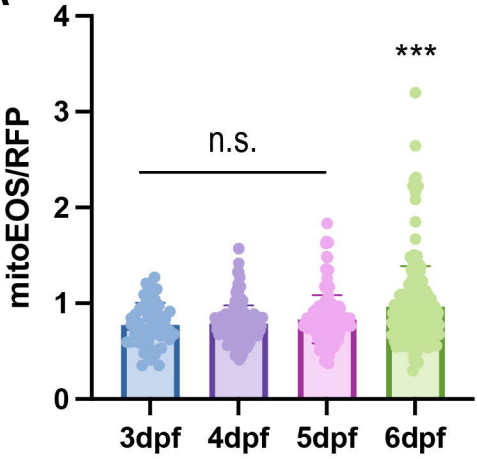
mitoEOS/RFP
4
3
2
1
0
n.s.
***
3dpf
4dpf
5dpf
6dpf

B

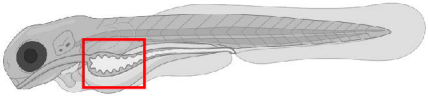

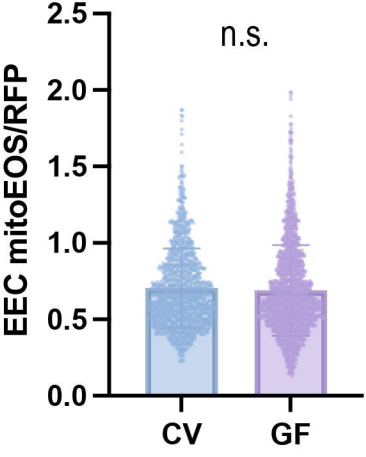
EEC mitoEOS/RFP
2.5
2.0
1.5
1.0
0.5
0.0
n.s.
CV
GF

C

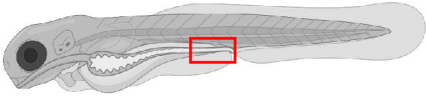

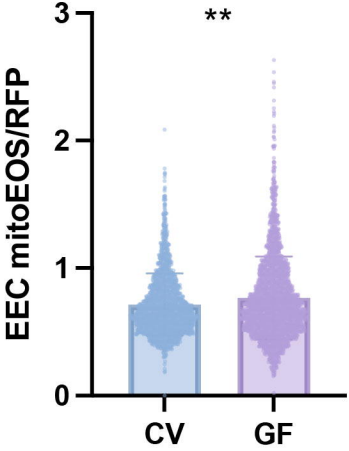
EEC mitoEOS/RFP
3
2
1
0
**
CV
GF

Linoleic acid increases EEC cytoplasmic and mitochondrial calcium

A

neurod1:Gcamp6f EEC cytoplasmid calcium
neurod1:mitoRGECO EEC mitochondrial calcium

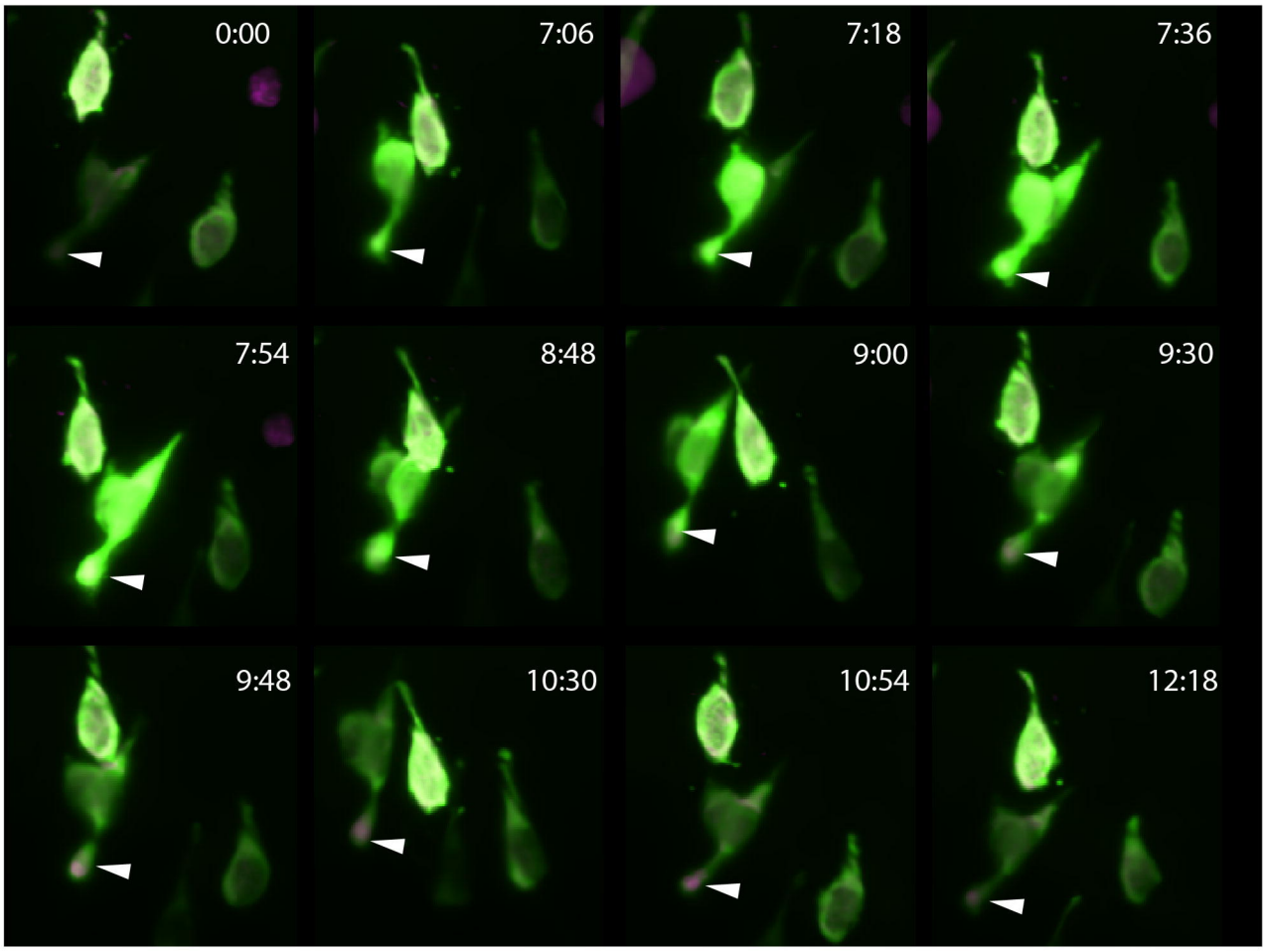

B

neurod1:mitoRGECO EEC mitochondrial calcium

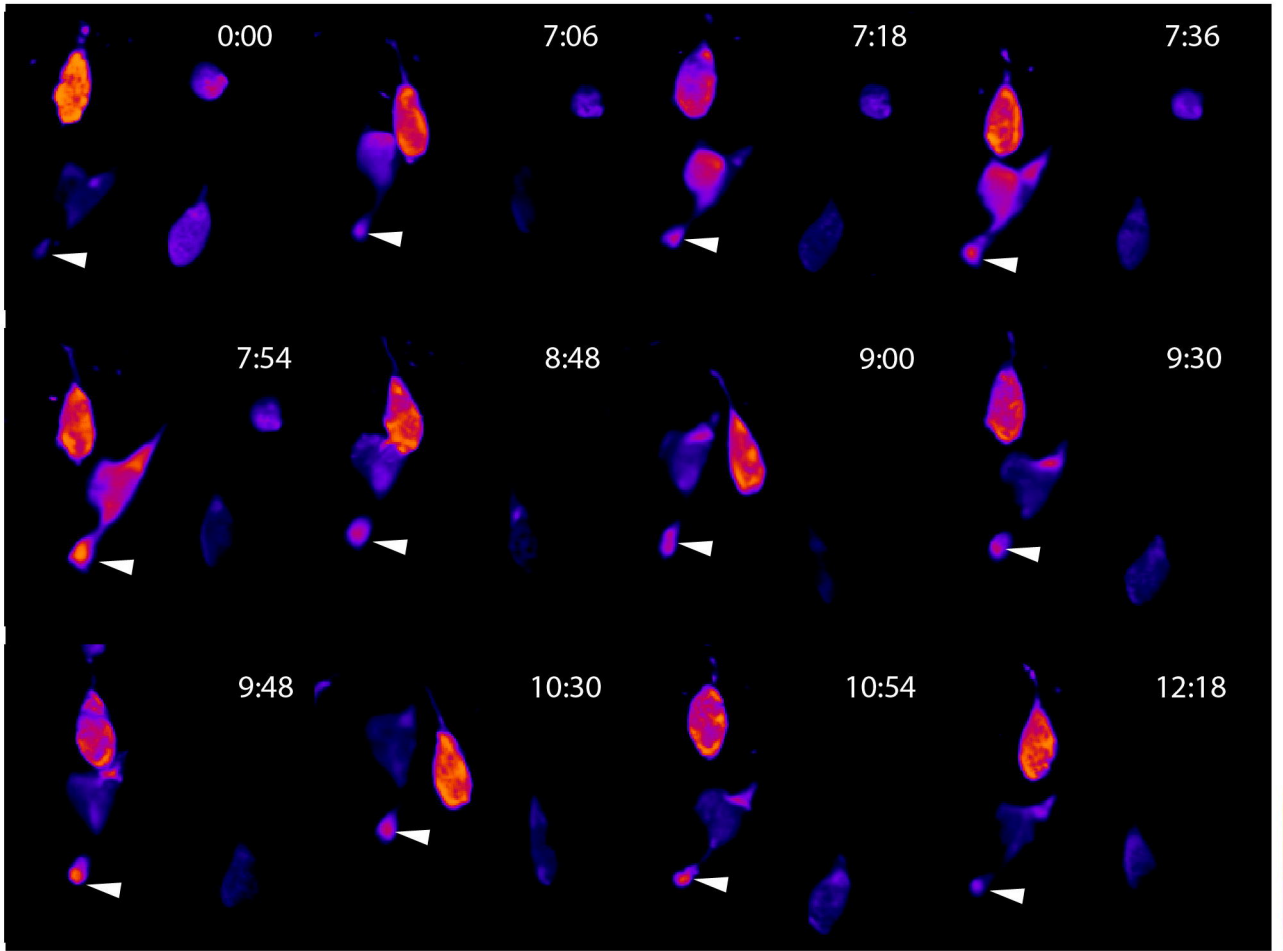

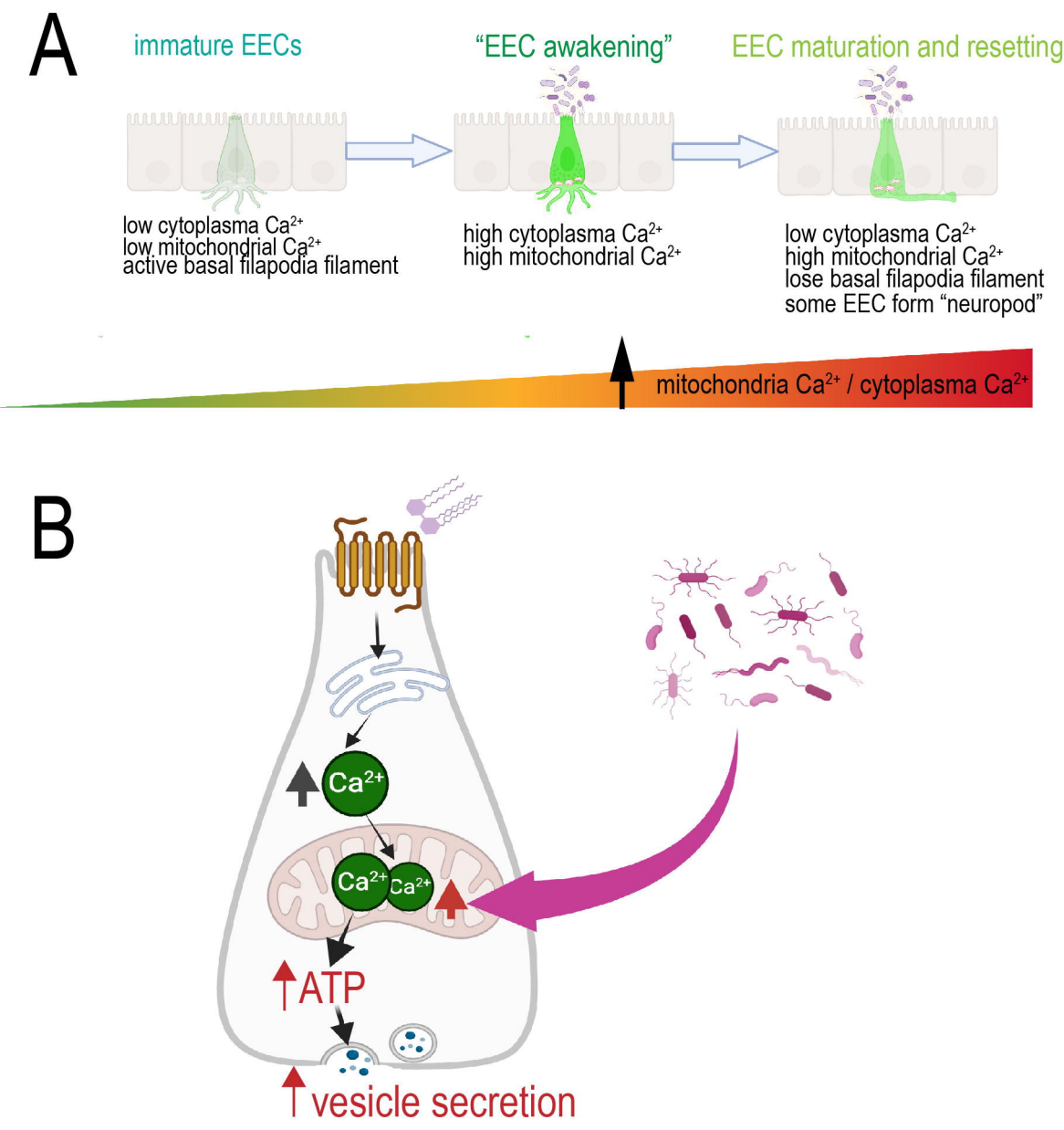
A
immature EECs
"EEC awakening"
EEC maturation and resetting
low cytoplasma Ca2+
low mitochondrial Ca2+
active basal filapodia filament
high cytoplasma Ca2+
high mitochondrial Ca2+
low cytoplasma Ca2+
high mitochondrial Ca2+
lose basal filapodia filament
some EEC form "neuropod"
mitochondria Ca2+ / cytoplasma Ca2+
B
Ca2+
Ca2+
Ca2+
ATP
vesicle secretion